Check for updates

Received: 27 July 2023 | Revised: 12 December 2023 | Accepted: 13 February 2024

IET Renewable Power Generation

DOI: 10.1049/rpg2.12974

The Institution of Engineering and Technology WILEY

ORIGINAL RESEARCH

Comparative analysis of the hybrid gazelle-Nelder–Mead algorithm for parameter extraction and optimization of solar photovoltaic systems

Serdar Ekinci[1] | **Davut Izci**[1] | **Abdelazim G. Hussien**[2,3,4,5]

[1]Department of Computer Engineering, Batman University, Batman, Turkey

[2]Department of Computer and Information Science, Linköping University, Linköping, Sweden

[3]Faculty of Science, Fayoum University, Fayoum, Egypt

[4]Applied Science Research Center, Applied Science Private University, Amman, Jordan

[5]MEU Research Unit, Middle East University, Amman, Jordan

Correspondence
Abdelazim G. Hussien, Applied Science Research Center, Applied Science Private University, Amman 11931, Jordan.
Email: aga08@fayoum.edu.eg; abdelazim.hussien@liu.se

Abstract

The pressing need for sustainable energy solutions has driven significant research in optimizing solar photovoltaic (PV) systems which is crucial for maximizing energy conversion efficiency. Here, a novel hybrid gazelle-Nelder–Mead (GOANM) algorithm is proposed and evaluated. The GOANM algorithm synergistically integrates the gazelle optimization algorithm (GOA) with the Nelder–Mead (NM) algorithm, offering an efficient and powerful approach for parameter extraction in solar PV models. This investigation involves a thorough assessment of the algorithm's performance across diverse benchmark functions, including unimodal, multimodal, fixed-dimensional multimodal, and CEC2020 benchmark functions. Notably, the GOANM consistently outperforms other optimization approaches, demonstrating enhanced convergence speed, accuracy, and reliability. Furthermore, the application of the GOANM is extended to the parameter extraction of the single diode and double diode models of RTC France solar cell and PV model of Photowatt-PWP201 PV module. The experimental results consistently demonstrate that the GOANM outperforms other optimization approaches in terms of accurate parameter estimation, low root mean square values, fast convergence, and alignment with experimental data. These results emphasize its role in achieving superior performance and efficiency in renewable energy systems.

1 | INTRODUCTION

In recent times, governments globally have heavily relied on fossil fuels to meet their electricity demands [1]. Unfortunately, this dependence has led to a significant increase in greenhouse gas emissions from thermal power plants, causing detrimental effects on human health and the environment over the past few decades [2]. Recognizing the critical impact of these environmental issues, scientists unanimously stress the importance of reducing dependence on fossil fuel combustion for electricity generation [3]. In response to these concerns, governments have proactively reassessed their energy policies and future investments, incorporating environmental considerations and promoting renewable energy sources as key solutions to transition towards a sustainable and eco-friendly energy model [4]. Various measures, including tax reductions/exemptions, policy initiatives, cost reductions, and the adoption of carbon taxes, have been implemented to pave the way for a brighter future that urgently addresses the need for sustainable energy while also considering economic factors. Solar energy has emerged as an exceptionally favourable option among these alternatives, thanks to its simplicity of implementation, ability to generate carbon-free electricity, widespread availability, and abundant presence on Earth's surface [5]. Solar energy technology finds practical applications in various fields [6–8], with solar photovoltaic (PV) systems, which directly convert solar energy into electricity, being widely employed. In the present era, the depletion of fossil fuel reserves at an alarming rate and growing ecological concerns have heightened the demand for renewable and environmentally friendly energy sources [9–11].

Parameter extraction is a crucial aspect when optimizing, simulating, and evaluating solar PV systems as it significantly

This is an open access article under the terms of the Creative Commons Attribution-NonCommercial-NoDerivs License, which permits use and distribution in any medium, provided the original work is properly cited, the use is non-commercial and no modifications or adaptations are made.
© 2024 The Authors. *IET Renewable Power Generation* published by John Wiley & Sons Ltd on behalf of The Institution of Engineering and Technology.

impacts the efficiency of converting solar energy into electricity [12–14]. Consequently, researchers have focused on studying methods to estimate solar cell parameters. Existing literature includes studies that employ various metaheuristic algorithms for forecasting these parameters [15–19]. For instance, the study in [20] addressed the challenge of accurately estimating model parameters for a PV cell in a PV generator, considering variations due to degradation and weather conditions. The latter study proposed particle swarm optimization with opposition-based initialization for parameter identification. The implementation of this method yielded promising results, offering a valuable approach for optimizing PV generating units. In [21], the researchers proposed the nutcracker optimizer. The study compared the performance using a silicon solar panel. The nutcracker optimizer outperformed other algorithms, exhibiting the best root mean square (RMSE) values in different diode models. Additionally, the proposed algorithm demonstrated the shortest average execution time, making it highly suitable for PV parameter extraction. In [22], the researchers introduced an improved artificial bee colony optimizer. They evaluated the algorithm using RMSE and mean absolute error, and showed it outperforms existing studies in terms of prediction accuracy. In [23], the growth optimization algorithm was introduced. The algorithm outperformed three contemporary techniques in terms of enhancing the electrical properties of PV systems and accurately determining unexplained PV parameters under various operating conditions. For the Kyocera KC200GT and RTC France PV modules, the proposed approach achieved significant improvements in performance compared to the other algorithms, demonstrating its effectiveness in optimizing solar energy conversion. The study in [24] employed the chimp optimizer and demonstrated its superior performance compared to existing algorithms in terms of durability, global search and convergence rate. The algorithm was evaluated using various PV modules and solar cells, including three commercially used modules, and the results confirmed its robustness and high performance in estimating parameters for different irradiance and temperature conditions. Apart from the above examples, different metaheuristic structures have also been employed to tackle the estimation of PV parameters [25–34].

Researchers have extensively explored the application of various metaheuristic algorithms to accurately estimate solar PV parameters, as evidenced by the existing literature. However, finding a robust and user-friendly optimizer is a challenging task that requires extensive research [35–38]. While these algorithms offer specific capabilities, there is still a need for optimization algorithms with high convergence ability to further enhance the performance of solar PV systems through parameter extraction. Hybridization presents a compelling solution to address the inherent challenges and complexities associated with conventional optimization approaches. By seamlessly integrating the strengths of multiple algorithms, hybridization not only enhances convergence speed but also ensures robustness, adaptability, and improved accuracy in parameter extraction for solar PV models. As solar energy technologies advance and system configurations become more intricate, the adoption of hybridization emerges as a strategic imperative to unlock the full potential of solar PV systems, pushing the boundaries of efficiency and contributing significantly to the sustainable future of renewable energy. This study therefore aims to address this challenge by conducting a comparative analysis of hybrid gazelle-Nelder–Mead (GOANM) algorithm in parameter extraction of PV model parameters of single diode model (SDM) and double diode model (DDM) of RTC France solar cell and Photowatt-PWP201 PV module. The integration of the Nelder-Mead (NM) algorithm [39] is performed in such a way that it improves the efficacy of the gazelle optimization algorithm (GOA) [40] while not causing a significant computational burden. In here, we employ NM algorithm as an aiding structure to improve the exploitation phase of a GOA. The intricate interplay between the GOA and the NM in the proposed GOANM algorithm stands as a testament to the efficacy of hybridization in achieving superior optimization results.

Initially, we used classical (unimodal, multimodal, fixed-dimensional multimodal) and CEC2020 benchmark functions as different test suites to assess the GOANM's performance. These benchmark functions hold immense significance as they serve as standard evaluation tools to gauge the efficacy of optimization algorithms. We compared the performance with the original GOA, which has already demonstrated efficiency compared to various other recent optimization algorithms [40]. The benchmark functions related experimental results demonstrate the superior performance of the GOANM. It consistently outperformed the original GOA in terms of achieving lower minimum values, exhibiting smaller standard deviations, and showcasing enhanced stability and reliability. These findings emphasize the effectiveness and superiority of proposed algorithms in tackling various types of optimization problems. We also presented the experimental results by employing the proposed approach for optimal solar PV models' parameters determination. The case studies selected for our analysis are the Photowatt-PWP201 and RTC France modules. These benchmarks were chosen as case studies due to their relevance in the field of solar photovoltaics. These case studies provide representative scenarios to evaluate the efficacy across different solar PV systems comparatively. Various analyses were employed to analyse and interpret the results, leading to meaningful conclusions about the efficacy of the proposed approach in optimizing PV models.

The experimental results of the SDM optimization using the GOANM showed higher accuracy in parameter estimation compared to the original GOA. The proposed algorithm consistently achieved lower RMSE values, indicating its superior performance in accurately estimating the I–V characteristics of the SDM. The convergence behaviour of the GOANM algorithm was faster and exhibited smoother convergence compared to GOA. The performance metrics of the GOANM algorithm showed close agreement between experimental and estimated values, demonstrating the accurate modelling capabilities of the proposed approach. The power–voltage (P–V) and current–voltage (I–V) curve characteristics of the optimized SDM using the GOANM algorithm closely matched the experimental data. Comparative analysis with other recent

17521424, 2024, 6, Downloaded from https://ietresearch.onlinelibrary.wiley.com/doi/10.1049/rpg2.12974 by Turkey Cochrane Evidence Aid, Wiley Online Library on [15/04/2025]. See the Terms and Conditions (https://onlinelibrary.wiley.com/terms-and-conditions) on Wiley Online Library for rules of use; OA articles are governed by the applicable Creative Commons License

optimization approaches (Gradient-based optimizer with Criss-cross and Nelder–Mead algorithm [41], local escape operators based improved moth flame algorithm [42], ranking teaching–learning-based algorithm [43], gradient based optimizer with differential evolution and sine cosine algorithm [44], dynamic leader multi-verse optimizer [45], reptile search algorithm with Cauchy mutation and opposition-based learning strategies [46], chaos game optimization-least squares [47], artificial humming bird optimization [48], particle swarm optimization with random reselection mechanism [49], elite learning adaptive differential evolution [50], coyote optimization algorithm [51], hunger games search with quantum Nelder–Mead [52], bald eagle search [53], tunicate swarm optimization [54], improved tree seed inspired algorithm [55], differential evolution [56]) further highlighted the GOANM's superior performance, as it achieved the lowest RMSE value among all the methods considered. Similar observations were made for the DDM optimization using the GOANM approach, indicating its effectiveness in fine-tuning the parameters of the DDM for the RTC France solar cell case study. The same observations were made for the Photowatt-PWP201 PV module. In light of the discussion so far, the contributions of this paper can be highlighted as follows:

- Introduction of the novel GOANM algorithm designed for precise parameter extraction in solar PV systems.
- Hybridization of the GOA and NM algorithm, offering a powerful and efficient approach that optimizes convergence speed, accuracy, and reliability.
- Comprehensive evaluation of the GOANM algorithm using a diverse set of benchmark functions, including unimodal, multimodal, fixed-dimensional multimodal, and CEC2020 benchmark functions, demonstrating its superiority over other optimization approaches.
- Extension of the GOANM algorithm's application to parameter extraction in solar PV models, specifically the SDM, DDM, and PV module models.
- Rigorous experimentation and statistical analyses confirming the GOANM algorithm's accuracy, efficiency, and reliability, contributing significantly to the advancement of optimization techniques in solar energy.
- Establishment of the GOANM algorithm's significance in optimizing solar PV systems, offering a pathway for enhanced efficiency and performance in renewable energy applications.

The rest of this paper is organized as follows. The subsequent section delves into a detailed review of related works, shedding light on the existing landscape of solar energy optimization and highlighting the gaps that our research aims to address. Following this, Section 3 provides an in-depth exposition of the GOANM algorithm, elucidating its underlying principles and the amalgamation of the GOA and NM algorithm. Section 4 introduces the benchmark functions, categorized into unimodal, multimodal, fixed-dimensional multimodal, and CEC2020 benchmark functions, serving as a comprehensive evaluation tool for assessing the performance of the GOANM algorithm. The experimental results and statistical analyses are presented in Section 5, showcasing the algorithm's prowess in optimizing solar PV models. Section 6 takes a closer look at the modelling aspects, specifically focusing on the SDM, DDM, and PV module models. Section 7 unveils the experimental results and statistical analyses of the parameter extraction process, offering insights into the accuracy and efficiency of the GOANM algorithm. Finally, Section 8 concludes the paper, summarizing key findings and proposing promising avenues for future research in the realm of solar energy optimization.

2 | OVERVIEW OF GAZELLE OPTIMIZATION ALGORITHM

The gazelle optimization algorithm (GOA) is inspired by the survival abilities of gazelles. It leverages the gazelles' adaptive characteristics, such as agility and speed, for real-world optimization problems [40]. Gazelles inhabit various regions and have evolved effective strategies, including leaping and running, to evade predators like cheetahs, jackals, and lions. This algorithm utilizes gazelles as search agents which are represented by a randomly initialized $n \times d$ matrix given in Equation (1). To establish the permissible range of values for the population vector, the algorithm integrates the constraints of upper bound (UB) and lower bound (LB).

$$X = \begin{bmatrix} x_{1,1} & x_{1,2} & \cdots & x_{1,d-1} & x_{1,d} \\ x_{2,1} & x_{2,2} & \cdots & x_{2,d-1} & x_{2,d} \\ \vdots & \vdots & x_{i,j} & \vdots & \vdots \\ x_{n,1} & x_{n,2} & \cdots & x_{n,d-1} & x_{n,d} \end{bmatrix} \tag{1}$$

Here, X represents the matrix of candidate population's position vectors. Equation (2) stochastically generates each position vector ($x_{i,j}$) where $rand$ denotes a random number, and UB_j and LB_j are the upper and lower bounds for the problem, respectively. The variables n and d represent the gazelle number and the dimension of the problem, respectively.

$$x_{i,j} = rand \times \left(UB_j - LB_j\right) + LB_j \tag{2}$$

In each iteration, $x_{i,j}$ generates a candidate solution, and the best solution obtained so far is identified as the minimum solution. In nature, the strongest or fittest gazelles have superior abilities in spotting threats, alerting others, and evading predators. Thus, the top gazelle is designated as the best-obtained solution which is used in Equation (3) to construct an Elite $n \times d$ matrix which serves as a reference for the gazelles to determine their next steps during the search process.

$$Elite = \begin{bmatrix} x'_{1,1} & x'_{1,2} & \cdots & x'_{1,d-1} & x'_{1,d} \\ x'_{2,1} & x'_{2,2} & \cdots & x'_{2,d-1} & x'_{2,d} \\ \vdots & \vdots & x'_{i,j} & \vdots & \vdots \\ x'_{n,1} & x'_{n,2} & \cdots & x'_{n,d-1} & x'_{n,d} \end{bmatrix} \tag{3}$$

17521424, 2024, 6, Downloaded from https://ietresearch.onlinelibrary.wiley.com/doi/10.1049/rpg2.12974 by Turkey Cochrane Evidence Aid, Wiley Online Library on [15/04/2025]. See the Terms and Conditions (https://onlinelibrary.wiley.com/terms-and-conditions) on Wiley Online Library for rules of use; OA articles are governed by the applicable Creative Commons License

Here, the position vector of the leading gazelle is denoted as $x'_{i,j}$. The GOA treats both predators and gazelles as search agents, as they both move in the same direction when a predator is detected, seeking safety. Consequently, while the gazelles flee, the predator also explores the search area. At the end of each iteration, the Elite matrix is updated if a better gazelle replaces the top gazelle.

The GOA emulates the gazelles' survival behaviour, encompassing grazing in the absence of predators and fleeing to a safe haven when a predator is detected. Therefore, the optimization process of the GOA algorithm can be divided into two distinct phases (exploitation and exploration). In the exploitation phase, the gazelles peacefully forage without a predator or in the presence of a stalking predator. To effectively explore the neighbouring areas of the domain, a controlled Brownian motion with uniform and controlled steps is employed. The displacement in a random motion is governed by the Gaussian (normal) probability distribution function with unit variance (σ^2) of 1 and mean (μ) of 0. At a given point x, the standard Brownian motion [57] is described by the following definition.

$$f_B(x,\mu,\sigma) = \frac{1}{\sqrt{2\pi\sigma^2}} e^{\left(-\frac{(x-\mu)^2}{2\sigma^2}\right)} = \frac{1}{\sqrt{2\pi}} e^{\left(-\frac{x^2}{2}\right)} \quad (4)$$

During grazing, a Brownian motion pattern is modelled for the movement of the gazelles. The mathematical model representing this behaviour is given by Equation (5).

$$gazelle_{i+1} = gazelle_i + s \cdot R * \cdot R_B * \cdot \left(Elite_i - R_B * \cdot gazelle_i\right) \quad (5)$$

In this context, $gazelle_{i+1}$ corresponds to the solution at the subsequent iteration, whereas $gazelle_i$ represents the solution at the current iteration. The parameter s signifies the grazing speed of the gazelles. R_B is a vector composed of random numbers simulating Brownian motion, and R is a vector containing uniform random numbers within the range of 0 to 1.

The exploration phase begins when a predator is spotted. In response to danger, gazelles exhibit various behaviours such as tail flicking, foot stomping, or stotting up to a height of 2 m, which is scaled to a value between 0 and 1. This phase of the algorithm incorporates the use of Lévy flight, which involves taking small steps interspersed with occasional long jumps. Equation (6) describes the Lévy distribution [58].

$$L(x_j) \approx \left|x_j\right|^{1-\alpha} \quad (6)$$

In this equation, x_j represents the flight distance, and α is the power-law exponent, constrained within the range (1,2]. The Lévy stable process, denoted as an integral in Equation (7) [59], is defined as follows:

$$f_L(x;\alpha,\gamma) = \frac{1}{\pi} \int_0^{\infty} exp\left(-\gamma q^{\alpha}\right) cos\left(qx\right) \delta q \quad (7)$$

Here, the motion is governed by the distribution index (α), and γ represents the scale unit. GOA utilizes an algorithm proposed by [59] to generate stable Lévy motion. The algorithm adopts α values ranging from 0.3 to 1.99, and its formulation is provided in Equation (8).

$$Levy(\alpha) = 0.05 \times \frac{x}{|y|^{\frac{1}{\alpha}}} \quad (8)$$

The variables α, x, and y are defined as follows: x follows a normal distribution with variance σ_x^2 and mean 0, y follows a normal distribution with variance σ_y^2 and mean 0, and α is set to 1.5. The values of σ_x and σ_y are calculated as: $\sigma_x = \left(\Gamma(1+\alpha)\sin(\pi\alpha/2)/(\Gamma((1+\alpha)/2)\alpha 2^{(\alpha-1/2)})\right)^{1/\alpha}$ and $\sigma_y = 1$ [60]. This technique has demonstrated improved searchability in optimization studies. When the predator is sighted, the gazelle initiates a run while the predator gives chase. Both runs involve sudden changes in direction, represented by the parameter μ. In this study, it is assumed that the change in direction occurs in every iteration, with the gazelle moving in one direction during odd iterations and the opposite direction during even iterations. The gazelle responds first, employing Lévy flight for its escape, while the predator initially uses Brownian motion before transitioning to Lévy flight. The gazelle's behaviour of spotting the predator is mathematically described in Equation (9).

$$\overrightarrow{gazelle_{i+1}} = \overrightarrow{gazelle_i} + S \cdot \mu \cdot \vec{R} * \cdot \overrightarrow{R_L} * \cdot \left(\overrightarrow{Elite_i} - \overrightarrow{R_L} * \cdot \overrightarrow{gazelle_i}\right) \quad (9)$$

Here, S represents the top speed that the gazelle can achieve, $\overrightarrow{R_L}$ is a Lévy distribution-based vector of random numbers. The mathematical model in Equation (10) describes the behaviour of the predator as it chases the gazelle.

$$\overrightarrow{gazelle_{i+1}} = \overrightarrow{gazelle_i} + S \cdot \mu \cdot CF * \cdot \overrightarrow{R_B} * \cdot \left(\overrightarrow{Elite_i} - \overrightarrow{R_L} * \cdot \overrightarrow{gazelle_i}\right) \quad (10)$$

In Equation (10), CF represents the cumulative effect of the predator, calculated as $CF = (1 - iter/iterMax)^{(2 * iter/iterMax)}$. The authors of a study on Mongolian Gazelles reported an annual survival rate of 0.66, implying that predators are successful in only 0.34 situations [61]. The predator success rate (PSR) has an impact on the gazelle's ability to escape and prevents local minima trapping. Equation (11) models the effect of PSR.

$$\overrightarrow{gazelle_{i+1}} = \begin{cases} \overrightarrow{gazelle_i} + CF\left[\overrightarrow{LB} + \vec{R} * \cdot \left(\overrightarrow{UB} - \overrightarrow{LB}\right)\right] * \cdot \vec{U}; if\ r \le PSRs \\ \overrightarrow{gazelle_i} + [PSRs(1-r) + r]\left(\overrightarrow{gazelle_{r1}} - \overrightarrow{gazelle_{r2}}\right); else \end{cases} \quad (11)$$

17521424, 2024, 6, Downloaded from https://ietresearch.onlinelibrary.wiley.com/doi/10.1049/rpg2.12974 by Turkey Cochrane Evidence Aid, Wiley Online Library on [15/04/2025]. See the Terms and Conditions (https://onlinelibrary.wiley.com/terms-and-conditions) on Wiley Online Library for rules of use; OA articles are governed by the applicable Creative Commons License

In Equation (11), $\vec{U}$ is a constructed binary vector generated by a random number r from the interval [0, 1], such that $\vec{U} = 0$ for $r < 0.34$; otherwise $\vec{U} = 1$. The gazelle matrix contains random indexes of $r1$ and $r2$.

3 | HYBRID GAZELLE-NELDER–MEAD ALGORITHM

The NM simplex method, also known as the NM algorithm, is a widely used optimization algorithm for finding the maximum or minimum of a cost function in multiple dimensions [62]. It is particularly effective when the objective function is non-linear and does not have explicit mathematical form or derivatives. The algorithm is based on the concept of a simplex, which is a geometrical shape that generalizes triangles to higher dimensions. In the context of the NM algorithm, a simplex refers to a set of $N + 1$ points in N-dimensional space, where N is the number of variables in the objective function. These points form a convex polytope with each point representing a candidate solution. The NM algorithm proceeds iteratively, continually refining the simplex towards the optimal solution converge. At each iteration, the algorithm evaluates the cost function at each of the $N + 1$ simplex vertices and sorts them based on their function values. The simplex is then updated through a series of geometric transformations.

The transformations performed by the NM algorithm include reflection, expansion, contraction, and shrinkage. These transformations are applied to the simplex vertices to explore the objective function landscape efficiently. The specific transformation used depends on the ordering of the vertices and their function values. If the reflected point (obtained by reflecting the worst vertex about the centroid of the remaining points) yields a better function value than the second-worst vertex, the reflected point is accepted, and the algorithm proceeds to the next iteration.

On the other hand, if the reflected point is worse than the second-worst vertex but better than the worst, an expansion transformation is performed to explore further along that direction. If the reflected point is worse than the worst vertex, the algorithm checks if it is better than the worst of all vertices. If it is, a contraction transformation is performed to explore closer to the better points. If the reflected point is worse than the worst vertex and all other vertices, a shrinkage transformation is applied to bring the simplex closer together. The NM algorithm continues iteratively until certain convergence criteria are met, such as reaching a maximum number of iterations, achieving a desired tolerance, or when the simplex becomes very small. The solution is determined by the final simplex vertex, which corresponds to the best function value.

One of the advantages of the NM algorithm is its simplicity and robustness. It can handle a wide range of optimization problems without requiring derivatives of the objective function. Therefore, it has been employed to improve the performance of different structures [63–68]. Considering the above-mentioned feature of the NM algorithm, this study employs it as an aiding structure to improve the exploitation phase of the GOA. Figure 1 provides a detailed process of the GOANM. The integration of the NM algorithm is performed in such a way that it can improve the efficacy of the GOA while not causing a significant computational burden. In the proposed hybrid version of the gazelle-Nelder–Mead (GOANM) algorithm, the original version of the GOA starts initially and updates the positions of the agents. After ten iterations, the found solution is used to create a simplex and the NM algorithm takes care of the further improvement. The progress of the NM algorithm takes place after each ten iterations, and it performs two times of the total number of iterations in each process. In this way a highly efficient algorithm is constructed for different PV cell models and modules parameters estimation.

4 | CLASSICAL AND RECENT CEC BENCHMARK FUNCTIONS

Benchmark functions play a crucial role in evaluating the effectiveness of optimization algorithms, serving as standard tools for assessment. We categorized these functions into four groups: unimodal, multimodal, fixed-dimensional multimodal, and the CEC2020 benchmark functions, each posing unique challenges.

The unimodal benchmark functions, F1–F7, play a crucial role in evaluating an algorithm's ability to converge to the global optimum. Details of those functions can be found in our previous studies [69–71]. With a single minimum point, these functions assess the algorithm's capacity to efficiently explore the search space and locate the global solution. The selection of unimodal benchmark functions in our evaluation allows us to examine the GOANM's performance in terms of global exploration and convergence.

The multimodal benchmark functions, F8–F13, present a formidable challenge to optimization algorithms as they possess multiple local optima. Evaluating algorithms on these functions enables us to assess their capability to navigate complex landscapes and escape local optima to find the global optimum. The inclusion of functions such as Schwefel, Rastrigin, Ackley, Griewank, Penalized, and Penalized2 [69–71] in evaluation allows us to thoroughly examine the GOANM algorithm's performance in terms of global optimization in the presence of multiple optima. Fixed-dimensional multimodal benchmark functions, F14–F23, provide a specific context for evaluating algorithms, where the dimensionality of the search space is predetermined. These functions simulate real-world scenarios where the problem space has a fixed number of dimensions. By including functions like Hartman 3, Hartman 6, Foxholes, Six-Hump Camel, Kowalik, Goldstein-Price, Branin, Shekel 10, Shekel 7, and Shekel 5 [69–71] in assessment, we can analyse the GOANM algorithm's performance in tackling fixed-dimensional multimodal problems, showcasing its effectiveness in various real-world optimization scenarios.

The CEC2020 benchmark functions, F24–F33, hold particular significance as they can be used to replicate real-world

17521424, 2024, 6, Downloaded from https://ietresearch.onlinelibrary.wiley.com/doi/10.1049/rpg2.12974 by Turkey Cochrane Evidence Aid, Wiley Online Library on [15/04/2025]. See the Terms and Conditions (https://onlinelibrary.wiley.com/terms-and-conditions) on Wiley Online Library for rules of use; OA articles are governed by the applicable Creative Commons License

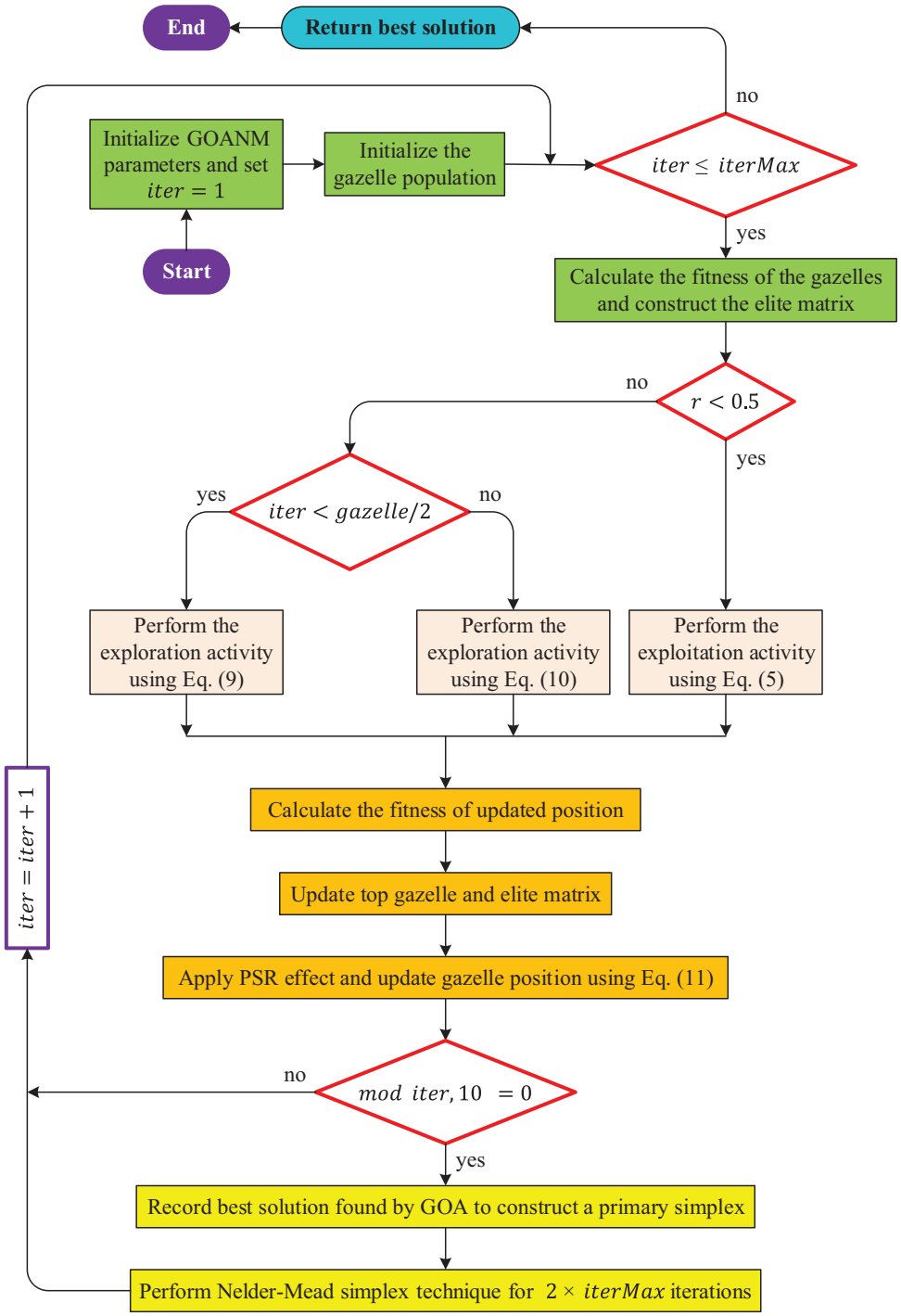


FIGURE 1 Hybrid gazelle-Nelder–Mead algorithm's process.

optimization challenges. These functions provide a rigorous evaluation platform, enabling algorithms to be tested on practical problem domains. By incorporating functions such as the shifted and rotated bent cigar, Schwefel's, Lunacek bi-Rastrigin, hybrid, expanded Rosenbrock's plus Griewangk's, and composition functions [72] in evaluation, we demonstrate the GOANM algorithm's competence in solving complex, real-world optimization problems.

By selecting benchmark functions across these categories, we comprehensively assess the GOANM algorithm's performance, gaining insights into its strengths and weaknesses in global exploration, local exploitation, handling multimodal landscapes, fixed-dimensional problems, and real-world optimization scenarios. This analysis provides a deeper understanding of the algorithm's robustness, versatility, and potential applicability across a broad spectrum of optimization problems.

17521424, 2024, 6, Downloaded from https://ietresearch.onlinelibrary.wiley.com/doi/10.1049/rpg2.12974 by Turkey Cochrane Evidence Aid, Wiley Online Library on [15/04/2025]. See the Terms and Conditions (https://onlinelibrary.wiley.com/terms-and-conditions) on Wiley Online Library for rules of use; OA articles are governed by the applicable Creative Commons License

TABLE 1 Unimodal benchmark functions related statistical results.

Function	Algorithm	Minimum	Average	Maximum	Standard deviation
F1	GOA	1.1883E−131	4.4512E−51	1.2859E−49	2.3463E−50
	GOANM	2.6682E−191	1.6783E−112	3.9178E−111	7.3700E−112
F2	GOA	3.4045E−79	6.9069E−29	9.7640E−28	2.3955E−28
	GOANM	3.9349E−100	2.3943E−68	7.1830E−67	1.3114E−67
F3	GOA	6.9254E−26	1.7035E−09	3.0767E−08	6.0608E−09
	GOANM	3.5706E−72	4.5170E−62	1.0417E−60	1.9051E−61
F4	GOA	3.2431E−41	1.8465E−10	4.8268E−09	8.8203E−10
	GOANM	4.5903E−85	2.1856E−52	6.5554E−51	1.1968E−51
F5	GOA	2.2082E+01	2.3264E+01	2.4540E+01	5.3442E−01
	GOANM	4.5921E−17	1.1454E−12	3.4347E−11	6.2708E−12
F6	GOA	1.2075E−03	1.4593E−02	4.4055E−02	1.1408E−02
	GOANM	5.2645E−18	1.4857E−17	3.0614E−17	6.4887E−18
F7	GOA	4.1019E−04	1.0919E−03	5.2536E−03	9.6583E−04
	GOANM	1.1389E−05	3.0329E−04	5.8977E−04	1.7792E−04

The presented values are in the standard presentation which is consistent with the literature.

5 | EXPERIMENTAL RESULT ON BENCHMARK FUNCTIONS

We compared the GOANM's performance with the original GOA, which has already demonstrated efficacy compared to various other optimization algorithms [40]. By comparing the statistical metrics between GOA and GOANM, we aim to highlight the superior performance of GOANM. The population size was set to 50 and the maximum number of iterations to 1000 and the algorithms were run 30 times. For the comparative evaluation, we employed the default parameters of GOA, specifically $S = 0.88$ and $PSR = 0.34$, and the default parameters of NM (for the GOANM), which are $\rho = 1$, $\gamma = 2$, $\beta = 0.5$, and $\delta = 0.5$. These parameter settings allow for a fair comparison between the two algorithms.

Table 1 summarizes the statistical outcomes from the unimodal benchmark functions, presenting minimum, maximum, average, and standard deviation values for both GOA and GOANM. Across all unimodal benchmark functions (F1–F7), it is evident that GOANM consistently outperforms GOA by attaining lower minimum values. Moreover, GOANM exhibits smaller standard deviations, indicating more reliable and consistent optimization results. These findings strongly suggest that GOANM is better equipped for tackling unimodal problems, showcasing enhanced convergence towards the global optimum.

Table 2 provides the statistical outcomes from the multimodal benchmark functions (F8–F13). Here, GOANM maintains its superior performance over GOA. In most instances, GOANM achieves lower minimum values, showcasing its superior ability to navigate away from local optima and discover the global optimum. Additionally, the generally smaller standard deviations of GOANM signify heightened stability and reliability throughout the optimization process. These results underscore the effectiveness of GOANM in addressing multimodal optimization problems.

Table 3 presents the statistical results obtained from the fixed-dimensional multimodal benchmark functions (F14–F23). For these functions, both GOA and GOANM exhibit identical minimum, maximum, and average values. However, GOANM consistently achieves a standard deviation of 0, indicating highly consistent and reproducible results. This suggests that GOANM has an inherent ability to converge to the same solution consistently for fixed-dimensional multimodal problems.

In Table 4, we present the statistical outcomes from the CEC2020 benchmark functions (F24–F33). Here, GOANM shines with its outstanding performance, securing lower minimum values compared to GOA. Furthermore, GOANM displays smaller standard deviations, indicating improved stability and reliability in pinpointing near-optimal solutions. These results vividly highlight GOANM's prowess in effectively addressing complex real-world optimization problems.

6 | SOLAR PV SYSTEM MODELING

6.1 | Single diode model

The single diode model (SDM) offers a simplified mathematical representation of the electrical characteristics exhibited by a PV cell. It assumes that the PV cell can be effectively modelled as a single diode connected in parallel with a current source. Despite its simplicity, the SDM manages to capture the essential aspects of the PV cell's electrical response while providing a computationally efficient representation. In the SDM, the I–V

17521424, 2024, 6, Downloaded from https://ietresearch.onlinelibrary.wiley.com/doi/10.1049/rpg2.12974 by Turkey Cochrane Evidence Aid, Wiley Online Library on [15/04/2025]. See the Terms and Conditions (https://onlinelibrary.wiley.com/terms-and-conditions) on Wiley Online Library for rules of use; OA articles are governed by the applicable Creative Commons License

TABLE 2 Multimodal benchmark functions related statistical results.

Function	Algorithm	Minimum	Average	Maximum	Standard deviation
$F8$	GOA	−1.0623E+04	−8.6395E+03	−7.2400E+03	9.2278E+02
	GOANM	−1.1866E+04	−1.0243E+04	−9.0685E+03	7.6658E+02
$F9$	GOA	0	0	0	0
	GOANM	0	0	0	0
$F10$	GOA	8.8818E−16	4.3225E−15	4.4409E−15	6.4863E−16
	GOANM	8.8818E−16	8.8818E−16	8.8818E−16	0
$F11$	GOA	0	0	0	0
	GOANM	0	0	0	0
$F12$	GOA	1.9353E−06	4.1417E−04	1.0736E−03	2.8723E−04
	GOANM	2.0707E−19	3.5953E−19	7.0830E−19	1.1335E−19
$F13$	GOA	3.3715E−04	1.5749E−02	7.9455E−02	1.9358E−02
	GOANM	2.4204E−18	5.1204E−18	9.9562E−18	1.8746E−18

The presented values are in the standard presentation which is consistent with the literature.

TABLE 3 Fixed-dimensional multimodal benchmark functions related statistical results.

Function	Algorithm	Minimum	Average	Maximum	Standard deviation
$F14$	GOA	9.9800E−01	9.9800E−01	9.9800E−01	0
	GOANM	9.9800E−01	9.9800E−01	9.9800E−01	0
$F15$	GOA	3.0749E−04	3.0749E−04	3.0749E−04	8.2901E−14
	GOANM	3.0749E−04	3.0749E−04	3.0749E−04	0
$F16$	GOA	−1.0316E+00	−1.0316E+00	−1.0316E+00	7.4015E−17
	GOANM	−1.0316E+00	−1.0316E+00	−1.0316E+00	0
$F17$	GOA	3.9789E−01	3.9789E−01	3.9789E−01	0
	GOANM	3.9789E−01	3.9789E−01	3.9789E−01	0
$F18$	GOA	3	3	3	1.3157E−15
	GOANM	3	3	3	0
$F19$	GOA	−3.8628E+00	−3.8628E+00	−3.8628E+00	9.3622E−16
	GOANM	−3.8628E+00	−3.8628E+00	−3.8628E+00	0
$F20$	GOA	−3.3220E+00	−3.3220E+00	−3.3220E+00	6.8404E−13
	GOANM	−3.3220E+00	−3.3220E+00	−3.3220E+00	0
$F21$	GOA	−1.0153E+01	−1.0153E+01	−1.0153E+01	2.1349E−15
	GOANM	−1.0153E+01	−1.0153E+01	−1.0153E+01	0
$F22$	GOA	−1.0403E+01	−1.0403E+01	−1.0403E+01	2.6480E−15
	GOANM	−1.0403E+01	−1.0403E+01	−1.0403E+01	0
$F23$	GOA	−1.0536E+01	−1.0536E+01	−1.0536E+01	2.9008E−15
	GOANM	−1.0536E+01	−1.0536E+01	−1.0536E+01	0

The presented values are in the standard presentation which is consistent with the literature.

relationship of a PV cell is defined by the following equation:

$$I = I_{ph} - I_{sd}\left[e^{\frac{(V+IR_s)}{(nV_t)}} - 1\right] - \frac{(V + IR_s)}{R_{sh}} \tag{12}$$

where I is the output current of the PV cell, V is the voltage across the PV cell terminals, I_{ph} is the photocurrent generated by the cell under illumination, I_{sd} is the diode saturation current, R_s is the series resistance of the cell, R_{sh} is the shunt resistance of the cell, n is the diode ideality factor, V_t is the thermal voltage, approximately equal to kT/q, where k is Boltzmann's constant, T is the temperature in Kelvin, and q is the elementary charge. Figure 2 illustrates the conceptual depiction of a solar PV cell employing the single-diode model.

17521424, 2024, 6, Downloaded from https://ietresearch.onlinelibrary.wiley.com/doi/10.1049/rpg2.12974 by Turkey Cochrane Evidence Aid, Wiley Online Library on [15/04/2025]. See the Terms and Conditions (https://onlinelibrary.wiley.com/terms-and-conditions) on Wiley Online Library for rules of use; OA articles are governed by the applicable Creative Commons License

TABLE 4 CEC2020 benchmark functions statistical results.

Function	Algorithm	Minimum	Average	Maximum	Standard deviation
F24	GOA	1.0003E+02	1.0057E+02	1.0197E+02	5.2301E−01
	GOANM	1.0000E+02	1.0000E+02	1.0000E+02	6.3443E−14
F25	GOA	1.1093E+03	1.2486E+03	1.4632E+03	1.1162E+02
	GOANM	1.1036E+03	1.1730E+03	1.2802E+03	6.2295E+01
F26	GOA	7.1430E+02	7.1871E+02	7.2286E+02	2.5137E+00
	GOANM	7.1189E+02	7.1623E+02	7.2106E+02	2.3041E+00
F27	GOA	1.9000E+03	1.9001E+03	1.9006E+03	2.0976E−01
	GOANM	1.9000E+03	1.9000E+03	1.9000E+03	0
F28	GOA	1.7251E+03	1.7597E+03	1.8000E+03	2.1296E+01
	GOANM	1.7014E+03	1.7155E+03	1.7382E+03	1.0756E+01
F29	GOA	1.6009E+03	1.6017E+03	1.6022E+03	3.0471E−01
	GOANM	1.6002E+03	1.6010E+03	1.6015E+03	2.8441E−01
F30	GOA	2.1024E+03	2.1086E+03	2.1203E+03	5.0900E+00
	GOANM	2.1004E+03	2.1018E+03	2.1048E+03	1.0957E+00
F31	GOA	2.2000E+03	2.2648E+03	2.3036E+03	4.9970E+01
	GOANM	2.2000E+03	2.2638E+03	2.3018E+03	4.6728E+01
F32	GOA	2.4179E+03	2.5384E+03	2.7379E+03	7.9717E+01
	GOANM	2.4007E+03	2.5172E+03	2.6038E+03	4.7026E+01
F33	GOA	2.6007E+03	2.8849E+03	2.8978E+03	5.6059E+01
	GOANM	2.6000E+03	2.8680E+03	2.8977E+03	9.0850E+01

The presented values are in the standard presentation which is consistent with the literature.

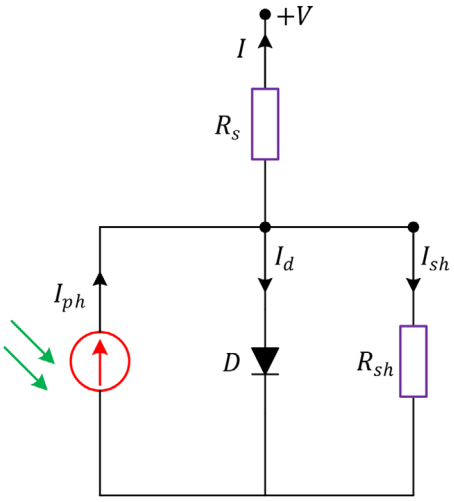


FIGURE 2 Single diode model equivalent circuit.

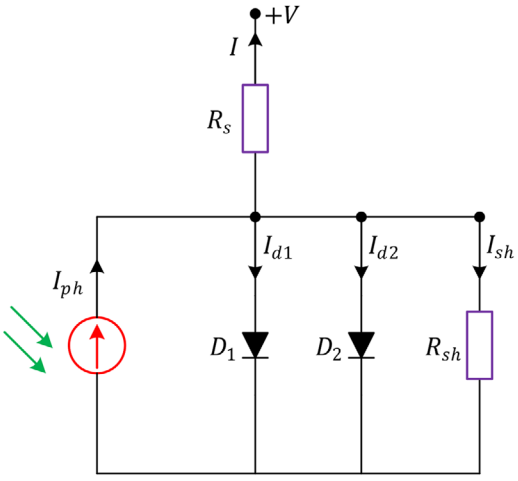


FIGURE 3 Double diode equivalent circuit.

6.2 | Double diode model

The double diode model (DDM) represents an advanced approach to PV cell modelling that incorporates additional diodes to capture more complex electrical behaviour. By introducing an extra diode to account for recombination losses within the PV cell, the DDM offers a more precise description of real-world PV cell characteristics. In the DDM, the *I*–*V* relationship of a PV cell is defined by the following equation:

$$I = I_{ph} - I_{sd1}\left[e^{\frac{(V+IR_s)}{(n_1 V_t)}} - 1\right] - I_{sd2}\left[e^{\frac{(V+IR_s)}{(n_2 V_t)}} - 1\right] - \frac{(V + IR_s)}{R_{sh}} \quad (13)$$

where I_{sd1} is the diode saturation current of the main diode, I_{sd2} is the diode saturation current of the additional diode, n_1 is the ideality factor of the main diode and n_2 is the ideality factor of the additional diode. Figure 3 illustrates the conceptual

17521424, 2024, 6, Downloaded from https://ietresearch.onlinelibrary.wiley.com/doi/10.1049/rpg2.12974 by Turkey Cochrane Evidence Aid, Wiley Online Library on [15/04/2025]. See the Terms and Conditions (https://onlinelibrary.wiley.com/terms-and-conditions) on Wiley Online Library for rules of use; OA articles are governed by the applicable Creative Commons License

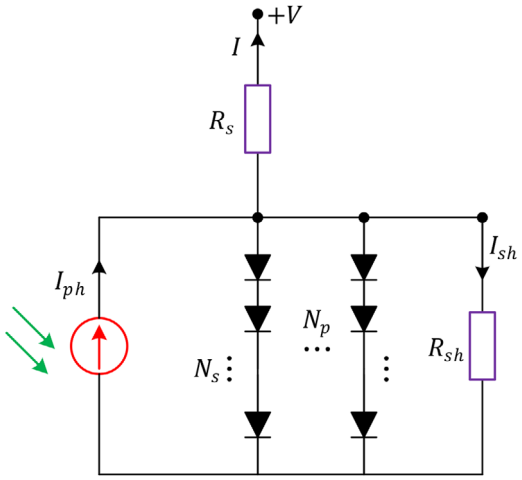


FIGURE 4 Photovoltaic module equivalent circuit.

depiction of a solar PV cell employing the double-diode model.

Compared to the SDM, the DDM offers a more accurate representation of the electrical characteristics of PV cells, particularly in situations where recombination losses significantly impact performance. However, due to the increased complexity of the model, parameter estimation for the DDM can be more computationally intensive and requires a larger number of measurement data points to achieve reliable results.

6.3 | Photovoltaic module model

The photovoltaic (PV) module model captures the relationship between the incident solar irradiance, temperature, and the electrical characteristics of the module. The related model is typically based on the equivalent circuit model, which represents the PV module as an electrical circuit with various components. The main components of the equivalent circuit model include a current source, a diode, a series resistance, and a shunt resistance. The model assumes that the PV module can be represented as a single diode connected in parallel with a current source. Figure 4 represents the equivalent circuit of a PV module where N_p and N_s are denoting the number of cells in parallel and series respectively. Since the solar cells are connected in series largely, the N_p value equals to 1. Therefore, the mathematical model of a PV module can be represented as follows:

$$I = I_{ph} - I_{sd}\left[e^{\frac{(V+IR_sN_s)}{(nN_sV_t)}} - 1\right] - \frac{(V + IR_sN_s)}{R_{sh}N_s} \tag{14}$$

6.4 | Objective function and proposed approach

During the cell parameter estimation process, an objective function plays a crucial role in quantifying estimated parameters' accuracy by comparing the modelled I–V curve with the measured data. RMSE is a commonly used objective function to assess the goodness-of-fit. RMSE, a widely used metric, quantifies the average magnitude of differences between the estimated (I_{est}) and experimentally measured (I_{exp}) values. The RMSE equation is as follows.

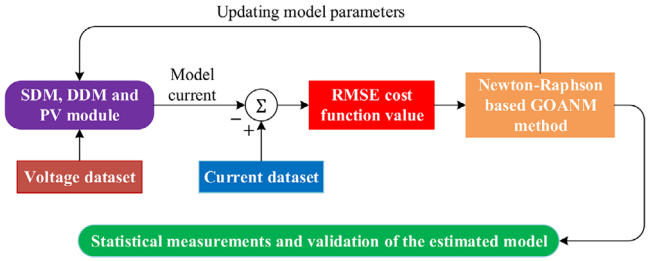


FIGURE 5 Parameter extraction process with the combination of Newton–Raphson method and Hybrid gazelle-Nelder–Mead algorithm.

$$RMSE = \sqrt{\frac{1}{N}\sum_{i=1}^{N}\left(I_{exp} - I_{est}\right)^2} \tag{15}$$

Here, N represents the total number of data points. RMSE provides a comprehensive measure of the overall discrepancy between the model and the measured data. By squaring the differences, RMSE penalizes larger errors more heavily, which can be beneficial when outliers or extreme values significantly impact the analysis. A lower RMSE value indicates better agreement between the model and the measurements.

For the parameter extraction in this study, we have chosen to utilize the iterative Newton–Raphson method [73]. This method offers notable advantages, including relatively low computational burden and high accuracy. The algorithm is implemented in conjunction with the Newton–Raphson method, ensuring their coordination throughout the process. Figure 5 illustrates the process of parameter extraction by combining the Newton–Raphson method with the GOANM algorithm.

7 | EXPERIMENTAL RESULTS AND STATISTICAL ANALYSIS

In this section, we present the experimental results and statistical analysis obtained by employing the recommended GOANM approach to determine the parameters of solar PV models. The analysis includes the Photowatt-PWP201 PV module and the RTC France solar cell as case studies. To ensure fairness and consistency, we set the population size to 30 and the maximum number of iterations to 400 for all experiments. Moreover, each case study was conducted 30 times to account for potential variations in the optimization process.

The utilization of the GOANM approach allowed us to explore the parameter space of the solar PV models systematically and efficiently. By integrating GOA with the NM algorithm, we were able to effectively fine-tune the parameters

17521424, 2024, 6, Downloaded from https://ietresearch.onlinelibrary.wiley.com/doi/10.1049/rpg2.12974 by Turkey Cochrane Evidence Aid, Wiley Online Library on [15/04/2025]. See the Terms and Conditions (https://onlinelibrary.wiley.com/terms-and-conditions) on Wiley Online Library for rules of use; OA articles are governed by the applicable Creative Commons License

TABLE 5 Boundaries (lower, upper) and single diode model's estimated parameters.

Parameter	*LB*	*UB*	Tuned by GOA	Tuned by GOANM
I_{ph} (A)	0	1	0.760696296925634	0.760787962711398
I_{sd} (A)	0	1	0.340007979124641	0.310690955651093
R_s (Ω)	0	0.5	0.036181834922442	0.036546780506234
R_{sh} (Ω)	0	100	55.702065611259407	52.889922116029553
n	1	2	1.486362887784568	1.477269734420784

The presented values are in the standard presentation which is consistent with the literature.

TABLE 6 Statistical RMSE values for single diode model obtained using gazelle optimization algorithm and hybrid gazelle-Nelder–Mead algorithm.

Algorithm	Minimum	Maximum	Average	Standard deviation
GOA	7.8704E−04	8.3108E−04	8.0358E−04	1.3714E−05
GOANM	7.7299E−04	7.7299E−04	7.7299E−04	1.8381E−09

The presented values are in the standard presentation which is consistent with the literature.

to maximize the performance of the models. The RTC France solar cell and Photowatt-PWP201 were chosen as benchmark case studies due to their relevance in the field of solar photovoltaics. These case studies provide representative scenarios to evaluate the effectiveness of the GOANM approach across different solar PV systems. Through the experimental runs, we collected a wealth of data regarding the optimized parameters and their corresponding performance metrics. We employed various statistical analysis techniques to analyse and interpret the results, enabling us to draw meaningful conclusions about the efficacy of the GOANM approach in optimizing solar PV models. In the subsequent sections, we present the detailed experimental setup, discuss the obtained results, and provide a comprehensive statistical analysis to evaluate the performance of the recommended GOANM approach in comparison to alternative methods.

7.1 | Experimental results of SDM and comparison with the more recent approaches

In this section, we present the experimental results of the single diode model optimization accomplished with the proposed GOANM approach. Furthermore, we conduct a comparison between the performance of our approach and other recent optimization algorithms for solar PV models. Table 5 showcases the estimated parameters of the SDM obtained using both the GOA and the GOANM algorithms. The results reveal that the GOANM algorithm achieves higher accuracy in parameter estimation compared to GOA. This underscores the superior performance of the proposed GOANM approach in fine-tuning the parameters of the SDM.

To further evaluate the performance of the GOANM algorithm, Table 6 presents the statistical RMSE values obtained for the single diode model using both GOA and GOANM. The

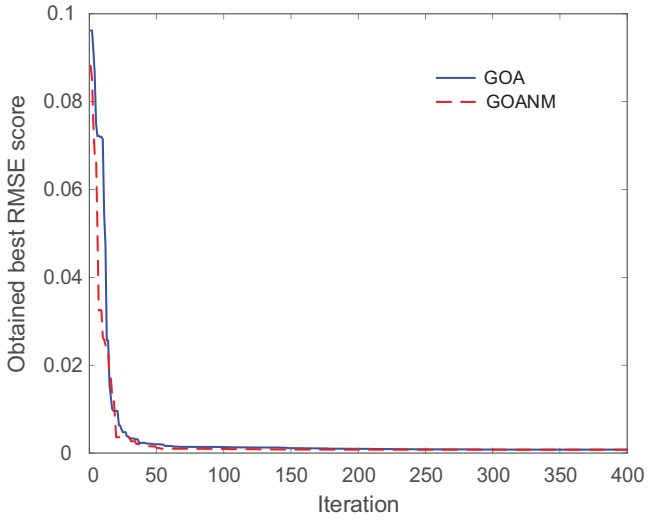


FIGURE 6 Convergence behaviour of gazelle optimization and hybrid gazelle-Nelder–Mead algorithms for single diode model.

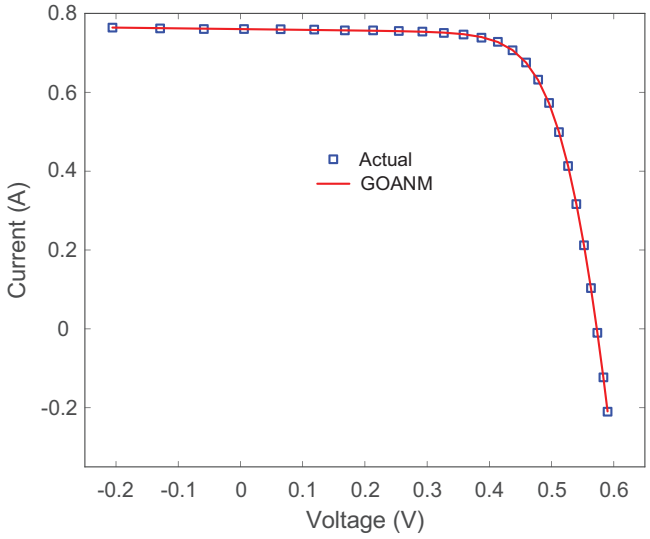


FIGURE 7 Single diode model current-voltage curve characteristics.

results demonstrate that the GOANM algorithm consistently achieved lower RMSE values compared to GOA. This indicates that the proposed GOANM approach can accurately estimate the *I–V* characteristics of the SDM, resulting in better model performance.

Figure 6 illustrates the convergence behaviour of the GOA and GOANM algorithms during the optimization process for the SDM. The figure demonstrates that the GOANM algorithm converges to a stable solution faster and exhibits smoother convergence behaviour compared to GOA. This further supports the effectiveness of the proposed GOANM approach.

Table 7 presents the performance metrics of the GOANM algorithm on the SDM, specifically for the RTC France solar cell case study. The results show a close agreement between the experimental and estimated values, indicating the accurate modelling capabilities of the GOANM. Furthermore, Figures 7

17521424, 2024, 6, Downloaded from https://ietresearch.onlinelibrary.wiley.com/doi/10.1049/rpg2.12974 by Turkey Cochrane Evidence Aid, Wiley Online Library on [15/04/2025]. See the Terms and Conditions (https://onlinelibrary.wiley.com/terms-and-conditions) on Wiley Online Library for rules of use; OA articles are governed by the applicable Creative Commons License

TABLE 7 SDM performance metrics of the hybrid gazelle-Nelder–Mead algorithm (RTC France solar cell).

No	V_{exp} (V)	I_{exp} (A)	I_{est} (A)	$\lvert I_{exp} - I_{est} \rvert$ (A)	P_{exp} (W)	P_{est} (W)	$\lvert P_{exp} - P_{est} \rvert$ (W)
#1	−0.2057	0.7640	0.7641	1.4945E−04	−0.1572	−0.1572	3.0743E−05
#2	−0.1291	0.7620	0.7627	7.0214E−04	−0.0984	−0.0985	9.0647E−05
#3	−0.0588	0.7605	0.7614	8.7377E−04	−0.0447	−0.0448	5.1378E−05
#4	0.0057	0.7605	0.7602	3.4550E−04	0.0043	0.0043	1.9693E−06
#5	0.0646	0.7600	0.7590	9.6095E−04	0.0491	0.0490	6.2077E−05
#6	0.1185	0.7590	0.7580	9.8924E−04	0.0899	0.0898	1.1723E−04
#7	0.1678	0.7570	0.7570	4.5703E−05	0.1270	0.1270	7.6689E−06
#8	0.2132	0.7570	0.7561	9.1517E−04	0.1614	0.1612	1.9511E−04
#9	0.2545	0.7555	0.7550	4.7765E−04	0.1923	0.1922	1.2156E−04
#10	0.2924	0.7540	0.7536	4.0264E−04	0.2205	0.2204	1.1773E−04
#11	0.3269	0.7505	0.7513	8.2726E−04	0.2453	0.2456	2.7043E−04
#12	0.3585	0.7465	0.7473	8.0533E−04	0.2676	0.2679	2.8871E−04
#13	0.3873	0.7385	0.7401	1.5846E−03	0.2860	0.2866	6.1372E−04
#14	0.4137	0.7280	0.7274	5.7385E−04	0.3012	0.3009	2.3740E−04
#15	0.4373	0.7065	0.7070	5.2588E−04	0.3090	0.3092	2.2997E−04
#16	0.4590	0.6755	0.6754	9.9737E−05	0.3101	0.3100	4.5779E−05
#17	0.4784	0.6320	0.6310	1.0019E−03	0.3023	0.3019	4.7930E−04
#18	0.4960	0.5730	0.5722	8.2531E−04	0.2842	0.2838	4.0935E−04
#19	0.5119	0.4990	0.4995	5.3894E−04	0.2554	0.2557	2.7589E−04
#20	0.5265	0.4130	0.4135	4.8481E−04	0.2174	0.2177	2.5525E−04
#21	0.5398	0.3165	0.3172	6.6147E−04	0.1708	0.1712	3.5706E−04
#22	0.5521	0.2120	0.2120	1.6519E−05	0.1170	0.1171	9.1200E−06
#23	0.5633	0.1035	0.1026	8.6345E−04	0.0583	0.0578	4.8638E−04
#24	0.5736	−0.0100	−0.0093	7.0131E−04	−0.0057	−0.0053	4.0227E−04
#25	0.5833	−0.1230	−0.1244	1.3616E−03	−0.0717	−0.0725	7.9422E−04
#26	0.5900	−0.2100	−0.2091	8.9768E−04	−0.1239	−0.1234	5.2963E−04
Total		$\sum_{i=1}^{N} \lvert I_{exp} - I_{est} \rvert = 0.017631844786274$			$\sum_{i=1}^{N} \lvert P_{exp} - P_{est} \rvert = 0.006480600926465$		

The presented values are in the standard presentation which is consistent with the literature.

and 8 illustrate the *I–V* and *P–V* curve characteristics, respectively, of the single diode model optimized using the GOANM algorithm. The figures demonstrate that the optimized model accurately captures the behaviour of the solar cell, as the curves closely match the experimental data.

To provide a comprehensive comparison, Table 8 compares the estimated parameters and RMSE values for the SDM obtained using the GOANM algorithm with other more recent optimization approaches, including gradient based optimizer with criss-cross and NM algorithms (CCNMGBO) [41], improved moth flame algorithm (IMFOL) [42], ranking teaching–learning-based optimization (RTLBO) [43], dynamic leader multi-verse optimizer (DLMVO) [45], reptile search algorithm with Cauchy mutation and opposition-based learning strategies (OBL-RSACM) [46], chaos game optimization-least squares (CGO-LS) [47], artificial humming bird optimization (AHO) [48], particle swarm optimization with random reselection (PSOCS) [49], elite learning adaptive differential evolution (ELADE) [50], coyote optimization algorithm (COA) [51], gradient based optimizer with differential evolution and sine cosine algorithm (SDGBO) [44], hunger games search algorithm with quantum Nelder–Mead (IHGS) [52], bald eagle search (BES) [53], differential evolution (DE) [56], improved tunicate swarm optimization (ITSA) [54], tree seed inspired algorithm (TSA) [55]. The results highlight the GOANM's superior performance, as it achieves the lowest RMSE value among all the compared methods. This emphasizes the significance of the proposed GOANM algorithm in accurately modelling the behaviour of the RTC France solar cell. In summary, the experimental results consistently demonstrate that the GOANM outperforms the other optimization approaches, as evidenced by its accurate parameter estimation, low RMSE values, fast convergence, and close alignment with the experimental data. These findings highlight the significance and efficacy of the GOANM in optimizing the SDM for solar PV systems, particularly for the RTC France solar cell case study.

17521424, 2024, 6, Downloaded from https://ietresearch.onlinelibrary.wiley.com/doi/10.1049/rpg2.12974 by Turkey Cochrane Evidence Aid, Wiley Online Library on [15/04/2025]. See the Terms and Conditions (https://onlinelibrary.wiley.com/terms-and-conditions) on Wiley Online Library for rules of use; OA articles are governed by the applicable Creative Commons License

TABLE 8 Single diode model estimated parameters and root mean square error values (RTC France solar cell).

Approach	I_{ph} (A)	I_{sd} (μA)	R_s (Ω)	R_{sh} (Ω)	n	*RMSE*
GOANM (proposed)	0.76079	0.31069	0.036547	52.8899	1.4773	**7.7299E−04**
GOA (proposed)	0.76070	0.34001	0.036182	55.7021	1.4864	7.8704E−04
CCNMGBO [41]	0.76078	0.323	0.036377	53.7185	1.4812	9.86E−04
IMFOL [42]	0.76078	0.32302	0.036377	53.7186	1.4812	9.8602E−04
RTLBO [43]	0.76078	0.32302	0.036377	53.7185	1.4812	9.8602E−04
DLMVO [45]	0.7608	0.3230	0.0364	53.7185	1.4812	9.8602E−04
OBL-RSACM [46]	0.76080	0.32203	0.03643	53.3521	1.4812	9.8452E−04
CGO-LS [47]	0.76078	0.32302	0.036377	53.7185	1.4812	9.8602E−04
AHO [48]	0.76079	0.31086	0.036540	52.8595	1.2155	7.7306E−04
PSOCS [49]	0.76078	0.32302	0.036377	53.719	1.4812	9.8602E−04
ELADE [50]	0.76078	0.32302	0.036377	53.7185	1.4812	9.8602E−04
COA [51]	0.76077	0.30839	0.036555	52.8267	1.4765	7.7547E−04
SDGBO [44]	0.76077	0.32302	0.036377	53.7185	1.4812	9.8602E−04
IHGS [52]	0.76078	0.32302	0.0364	53.7178	1.4812	9.8602E−04
BES [53]	0.7607	0.3230	0.0364	53.7185	1.4812	9.8602E−04
DE [56]	0.7607	0.3209	0.0363	54.1134	1.4709	7.7692E−04
ITSA [54]	0.7683	0.3262	0.0367	54.2557	1.4958	9.86E−04
TSA [55]	0.7606	0.3298	0.0363	56.5694	1.4832	9.9339E−04

The presented values are in the standard presentation which is consistent with the literature.

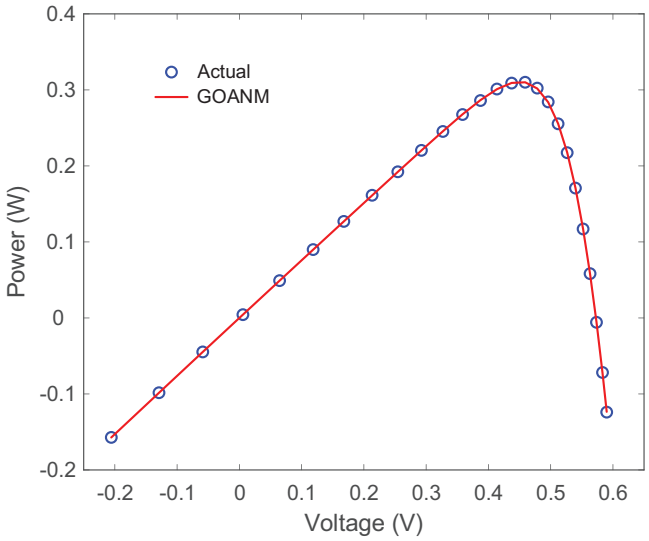


FIGURE 8 Single diode model power-voltage curve characteristics.

7.2 | Experimental results of DDM and comparison with the more recent approaches

In this section, we present the experimental results of the DDM optimization using the proposed GOANM approach. We also compare the performance of our approach with other more recent optimization algorithms for solar PV models. Table 9 provides the estimated parameters of the DDM obtained using both the GOA and the GOANM algorithms. The results show that the GOANM algorithm achieved a higher accuracy in parameter estimation compared to GOA. This indicates the superior performance of the proposed GOANM approach in fine-tuning the parameters of the DDM.

TABLE 9 Boundaries (lower, upper) and double diode model estimated parameters.

Parameter	*LB*	*UB*	Tuned by GOA	Tuned by GOANM
I_{ph} (A)	0	1	0.760791286994499	0.760808531034952
I_{sd1} (μA)	0	1	0.197041567273546	0.116241661477633
I_{sd2} (μA)	0	1	0.435630677002861	0.976797195739704
R_s (Ω)	0	0.5	0.036879911938545	0.037458928749482
R_{sh} (Ω)	0	100	54.261587214593369	55.729750829715613
n_1	1	2	1.441681765471988	1.399359428808557
n_2	1	2	1.818570007392350	1.859723442831997

The presented values are in the standard presentation which is consistent with the literature.

To further evaluate the performance of the GOANM algorithm, Table 10 presents the statistical RMSE values obtained for the double diode model using both GOA and GOANM. The results demonstrate that the GOANM algorithm consistently achieved lower RMSE values compared to GOA. This indicates that the proposed GOANM approach can accurately estimate the *I–V* characteristics of the DDM, resulting in better model performance.

Figure 9 illustrates the convergence behaviour of the GOA and GOANM algorithms during the optimization process for the DDM. The figure demonstrates that the GOANM

17521424, 2024, 6, Downloaded from https://ietresearch.onlinelibrary.wiley.com/doi/10.1049/rpg2.12974 by Turkey Cochrane Evidence Aid, Wiley Online Library on [15/04/2025]. See the Terms and Conditions (https://onlinelibrary.wiley.com/terms-and-conditions) on Wiley Online Library for rules of use; OA articles are governed by the applicable Creative Commons License

TABLE 10 Statistical root mean square error values for double diode model obtained using gazelle optimization algorithm and hybrid gazelle-Nelder–Mead algorithm.

Algorithm	Minimum	Maximum	Average	Standard deviation
GOA	7.5810E−04	8.8385E−04	7.7695E−04	2.4314E−05
GOANM	7.4339E−04	7.6714E−04	7.5263E−04	7.3732E−06

The presented values are in the standard presentation which is consistent with the literature.

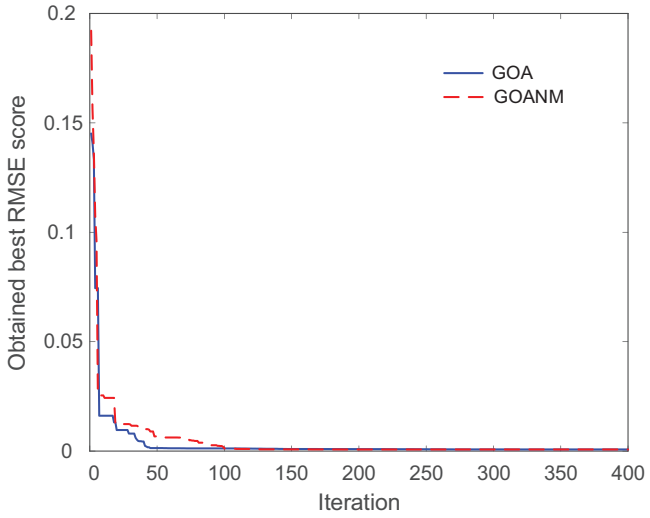


FIGURE 9 Convergence behaviour of gazelle optimization and hybrid gazelle-Nelder–Mead algorithms for double diode model.

algorithm converges to a stable solution faster and exhibits smoother convergence behaviour compared to GOA. This further supports the effectiveness and efficiency of the proposed GOANM approach.

Table 11 presents the performance metrics of the GOANM algorithm on the DDM, specifically for the RTC France solar cell case study. The results show a close agreement between the experimental and estimated values, indicating the accurate modelling capabilities of the GOANM algorithm. Furthermore, Figures 10 and 11 illustrate the I–V and P–V curve characteristics, respectively, of the DDM optimized using the GOANM algorithm. The figures demonstrate that the optimized model accurately captures the behaviour of the solar cell, as the curves closely match the experimental data.

To provide a comprehensive comparison, Table 12 compares the estimated parameters and RMSE values for the double diode model obtained using the GOANM algorithm with other more recent optimization approaches, including CCNMGBO [41], IMFOL [42], RTLBO [43], DLMVO [45], OBL-RSACM [46], CGO-LS [47], AHO [48], PSOCS [49], ELADE [50], COA [51], SDGBO [44], IHGS [52], BES [53], DE [56], ITSA [54], TSA [55]. The results highlight the GOANM's superior performance, as it achieves the lowest RMSE value among all the compared methods. This emphasizes the significance of the proposed

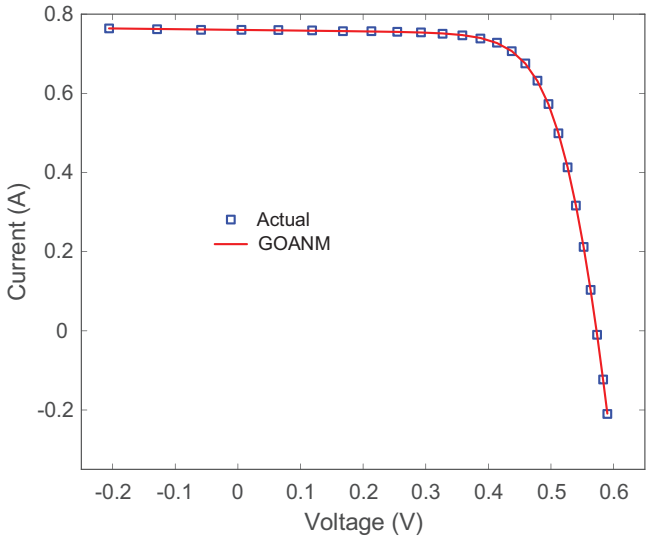


FIGURE 10 Double diode current-voltage curve characteristics.

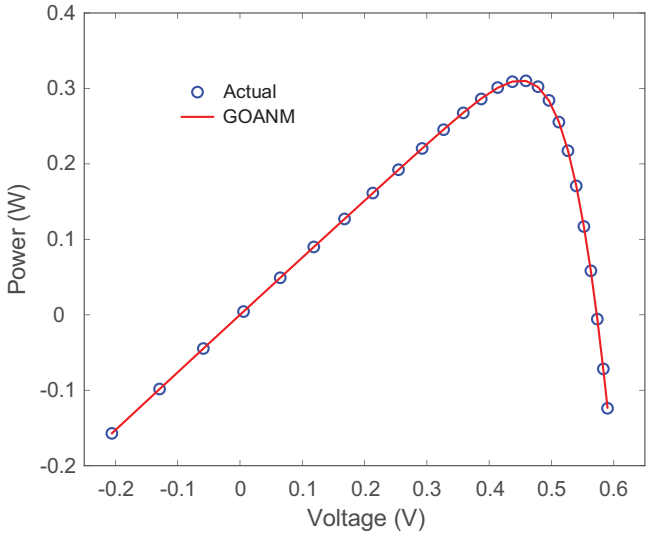


FIGURE 11 Double diode model power-voltage curve characteristics.

GOANM algorithm in accurately modelling the behaviour of the RTC France solar cell using the DDM.

7.3 | Experimental results of PV module and comparison with the more recent approaches

In this section, we present the experimental results of the photovoltaic module optimization using the proposed GOANM approach. We also compare the performance of our approach with other more recent optimization algorithms for PV modules. Table 13 provides the estimated parameters of the PV module obtained using both the GOA and the GOANM algorithms. The results indicate that the GOANM algorithm achieved a higher accuracy in parameter estimation compared

17521424, 2024, 6, Downloaded from https://ietresearch.onlinelibrary.wiley.com/doi/10.1049/rpg2.12974 by Turkey Cochrane Evidence Aid, Wiley Online Library on [15/04/2025]. See the Terms and Conditions (https://onlinelibrary.wiley.com/terms-and-conditions) on Wiley Online Library for rules of use; OA articles are governed by the applicable Creative Commons License

TABLE 11 Double diode model performance metrics of the hybrid gazelle-Nelder–Mead algorithm (RTC France solar cell).

No	V_{exp} (V)	I_{exp} (A)	I_{est} (A)	$\lvert I_{exp} - I_{est} \rvert$ (A)	P_{exp} (W)	P_{est} (W)	$\lvert P_{exp} - P_{est} \rvert$ (W)
#1	−0.2057	0.7640	0.7640	1.2893E−05	−0.1572	−0.1572	2.6521E−06
#2	−0.1291	0.7620	0.7626	6.1343E−04	−0.0984	−0.0985	7.9194E−05
#3	−0.0588	0.7605	0.7614	8.5239E−04	−0.0447	−0.0448	5.0121E−05
#4	0.0057	0.7605	0.7602	3.0588E−04	0.0043	0.0043	1.7435E−06
#5	0.0646	0.7600	0.7591	8.6775E−04	0.0491	0.0490	5.6056E−05
#6	0.1185	0.7590	0.7581	8.5202E−04	0.0899	0.0898	1.0096E−04
#7	0.1678	0.7570	0.7572	2.1286E−04	0.1270	0.1271	3.5718E−05
#8	0.2132	0.7570	0.7563	7.3916E−04	0.1614	0.1612	1.5759E−04
#9	0.2545	0.7555	0.7552	3.2242E−04	0.1923	0.1922	8.2056E−05
#10	0.2924	0.7540	0.7537	3.0405E−04	0.2205	0.2204	8.8905E−05
#11	0.3269	0.7505	0.7513	8.3592E−04	0.2453	0.2456	2.7326E−04
#12	0.3585	0.7465	0.7472	7.0670E−04	0.2676	0.2679	2.5335E−04
#13	0.3873	0.7385	0.7399	1.3940E−03	0.2860	0.2866	5.3990E−04
#14	0.4137	0.7280	0.7272	8.0180E−04	0.3012	0.3008	3.3170E−04
#15	0.4373	0.7065	0.7068	3.4092E−04	0.3090	0.3091	1.4909E−04
#16	0.4590	0.6755	0.6753	1.7037E−04	0.3101	0.3100	7.8199E−05
#17	0.4784	0.6320	0.6311	9.3872E−04	0.3023	0.3019	4.4908E−04
#18	0.4960	0.5730	0.5723	6.7020E−04	0.2842	0.2839	3.3242E−04
#19	0.5119	0.4990	0.4997	7.0433E−04	0.2554	0.2558	3.6055E−04
#20	0.5265	0.4130	0.4136	5.8094E−04	0.2174	0.2178	3.0586E−04
#21	0.5398	0.3165	0.3171	6.4668E−04	0.1708	0.1712	3.4908E−04
#22	0.5521	0.2120	0.2119	1.0027E−04	0.1170	0.1170	5.5357E−05
#23	0.5633	0.1035	0.1025	1.0253E−03	0.0583	0.0577	5.7754E−04
#24	0.5736	−0.0100	−0.0094	5.8055E−04	−0.0057	−0.0054	3.3300E−04
#25	0.5833	−0.1230	−0.1243	1.3368E−03	−0.0717	−0.0725	7.7973E−04
#26	0.5900	−0.2100	−0.2089	1.0990E−03	−0.1239	−0.1233	6.4839E−04
Total		$\sum_{i=1}^{N} \lvert I_{exp} - I_{est} \rvert = 0.017015244110354$			$\sum_{i=1}^{N} \lvert P_{exp} - P_{est} \rvert = 0.006471506735184$		

The presented values are in the standard presentation which is consistent with the literature.

to GOA. This suggests that the proposed GOANM approach is effective in fine-tuning the parameters of the PV module.

To further evaluate the performance, Table 14 presents the statistical RMSE values obtained for the PV module using both GOA and GOANM. The results show that the GOANM algorithm consistently achieved lower RMSE values compared to GOA. This indicates that the proposed GOANM approach accurately captures the current–voltage characteristics of the PV module, resulting in improved model performance.

Figure 12 illustrates the convergence behaviour of the GOA and GOANM algorithms during the optimization process for the PV module. The figure shows that the GOANM algorithm converges to a stable solution faster and exhibits smoother convergence behaviour compared to GOA. This demonstrates the effectiveness and efficiency of the proposed GOANM approach.

Table 15 presents the performance metrics of the GOANM algorithm on the PV module, specifically for the Photowatt-PWP201 case study. The results indicate a close agreement between the experimental and estimated values, indicating the accurate modelling capabilities of the GOANM algorithm for the PV module. Furthermore, Figures 13 and 14 illustrate the *I–V* and *P–V* curve characteristics, respectively, of the PV module optimized using the GOANM algorithm. The figures demonstrate that the optimized model closely matches the experimental data, accurately representing the behaviour of the PV module.

Table 16 provides a comparison of the estimated parameters and RMSE values for the PV module obtained using the GOANM algorithm with other more recent optimization approaches, including CCNMGBO [41], IMFOL [42], RTLBO [43], DLMVO [45], OBL-RSACM [46], CGO-LS [47], AHO [48], PSOCS [49], ELADE [50], COA [51], SDGBO [44], IHGS [52], BES [53], DE [56], ITSA [54], TSA [55]. The results show that the GOANM algorithm achieves the lowest RMSE value among the compared methods, indicating its superior performance in accurately modelling the Photowatt-PWP201 PV module.

17521424, 2024, 6, Downloaded from https://ietresearch.onlinelibrary.wiley.com/doi/10.1049/rpg2.12974 by Turkey Cochrane Evidence Aid, Wiley Online Library on [15/04/2025]. See the Terms and Conditions (https://onlinelibrary.wiley.com/terms-and-conditions) on Wiley Online Library for rules of use; OA articles are governed by the applicable Creative Commons License

TABLE 12 Double diode model estimated parameters and root mean square error values (RTC France solar cell).

Approach	I_{ph} (A)	I_{sd1} (μA)	I_{sd2} (μA)	R_s (Ω)	R_{sh} (Ω)	n_1	n_2	*RMSE*
GOANM (proposed)	0.76081	0.11624	0.9768	0.037459	55.7298	1.3994	1.8597	**7.4339E−04**
GOA (proposed)	0.76079	0.19704	0.4356	0.03688	54.2616	1.4417	1.8186	7.5810E−04
CCNMGBO [41]	0.76078	0.256	0.507	0.036609	54.9169	1.4613	2.0000	9.8200E−04
IMFOL [42]	0.76078	0.76632	0.2251	0.036731	55.6567	2.0000	1.4508	9.8252E−04
RTLBO [43]	0.76078	0.22597	0.7494	0.03674	55.4855	1.4510	2.0000	9.8248E−04
DLMVO [45]	0.7608	0.7493	0.2260	0.0367	55.4854	2.0000	1.4510	9.8248E−04
OBL-RSACM [46]	0.76033	0.39986	0.2677	0.03669	56.0102	1.4151	2.0000	9.8237E−04
CGO-LS [47]	0.76078	0.74935	0.2260	0.036740	55.4854	2.0000	1.4510	9.8248E−04
AHO [48]	0.76078	0.27988	0.2768	0.036530	54.2856	1.9563	1.4682	9.8401E−04
PSOCS [49]	0.76078	1.0000	0.1981	0.036874	56.172	2.0000	1.4401	9.8297E−04
ELADE [50]	0.76078	0.22598	0.7493	0.036740	55.4855	1.4510	2.0000	9.8248E−04
COA [51]	0.76072	0.24468	0.3802	0.036927	53.5130	1.4564	1.9899	7.6480E−04
SDGBO [44]	0.76078	0.50569	0.2557	0.036609	54.9246	2.0000	1.4614	9.8270E−04
IHGS [52]	0.76078	0.74935	0.2260	0.03674	55.48542	2.0000	1.45102	9.8248E−04
BES [53]	0.7608	0.2259	0.7493	0.0367	55.4854	1.4510	2.0000	9.8248E−04
DE [56]	0.7605	0.42322	0.1873	0.02061	51.9345	1.8758	1.4360	7.6300E−04
ITSA [54]	0.7608	0.9731	0.1679	0.0369	53.8368	1.9213	1.4281	9.82E−04
TSA [55]	0.7609	0.21658	0.2674	0.0367	52.5696	1.4503	1.7552	9.8894E−04

The presented values are in the standard presentation which is consistent with the literature.

TABLE 13 Boundaries (lower, upper) and photovoltaic module's estimated parameters.

Parameter	*LB*	*UB*	Tuned by GOA	Tuned by GOANM
I_{ph} (A)	0	2	1.029932680760576	1.031434032536007
I_{sd} (μA)	0	50	3.278277716184132	2.637962217404928
R_s (Ω)	0	2	1.212711988983959	1.235639579656891
R_{sh} (Ω)	0	2000	1046.586679976497	821.6098298498825
n	1	50	48.407643957435802	47.598052111668181

The presented values are in the standard presentation which is consistent with the literature.

TABLE 14 Statistical root mean square error values for photovoltaic module obtained using gazelle optimization algorithm and hybrid gazelle-Nelder–Mead algorithm.

Algorithm	Minimum	Maximum	Average	Standard deviation
GOA	2.1097E−03	2.3915E−03	2.2076E−03	7.9125E−05
GOANM	2.0528E−03	2.0528E−03	2.0528E−03	5.7403E−13

The presented values are in the standard presentation which is consistent with the literature.

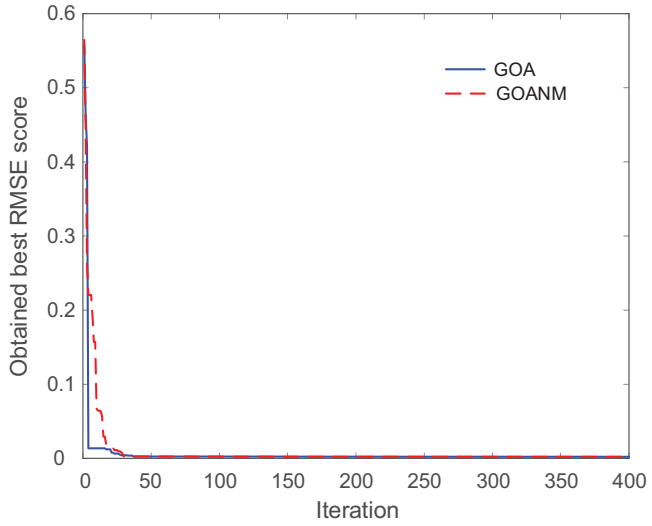


FIGURE 12 Convergence behaviour of gazelle optimizaiton and hybrid gazelle-Nelder–Mead algorithms for photovoltaic module.

8 | CONCLUSION

The contemporary overreliance on fossil fuels for electricity generation has prompted a surge in greenhouse gas emissions, necessitating a shift towards sustainable energy sources. Solar energy emerges as a compelling alternative, given its accessibility, eco-friendliness, and simplicity. Efficient solar PV systems demand precise parameter extraction, leading to the exploration of metaheuristic algorithms. Addressing the need for enhanced convergence ability in solar PV optimization, this study introduces and evaluates the GOANM algorithm. Combining the strengths of GOA and NM, GOANM consistently outperforms existing algorithms, exhibiting lower minimum values, reduced standard deviations, and heightened stability unimodal, multimodal, fixed-dimensional multimodal, and the CEC2020 benchmark functions. Applied to solar PV models, GOANM

17521424, 2024, 6, Downloaded from https://ietresearch.onlinelibrary.wiley.com/doi/10.1049/rpg2.12974 by Turkey Cochrane Evidence Aid, Wiley Online Library on [15/04/2025]. See the Terms and Conditions (https://onlinelibrary.wiley.com/terms-and-conditions) on Wiley Online Library for rules of use; OA articles are governed by the applicable Creative Commons License

TABLE 15 Performance metrics of the hybrid gazelle-Nelder–Mead algorithm on photovoltaic module (Photowatt-PWP201).

No.	V_{exp} (V)	I_{exp} (A)	I_{est} (A)	$\lvert I_{exp} - I_{est} \rvert$ (A)	P_{exp} (W)	P_{est} (W)	$\lvert P_{exp} - P_{est} \rvert$ (W)
#1	0.1248	1.0315	1.0297	1.7716E−03	0.1287	0.1285	2.2109E−04
#2	1.8093	1.0300	1.0277	2.3389E−03	1.8636	1.8593	4.2318E−03
#3	3.3511	1.0260	1.0257	2.7549E−04	3.4382	3.4373	9.2321E−04
#4	4.7622	1.0220	1.0238	1.8333E−03	4.8670	4.8757	8.7306E−03
#5	6.0538	1.0180	1.0218	3.8136E−03	6.1628	6.1859	2.3087E−02
#6	7.2364	1.0155	1.0193	3.8229E−03	7.3486	7.3762	2.7664E−02
#7	8.3189	1.0140	1.0157	1.7332E−03	8.4354	8.4498	1.4418E−02
#8	9.3097	1.0100	1.0100	2.1539E−05	9.4028	9.4026	2.0052E−04
#9	10.2163	1.0035	1.0004	3.0906E−03	10.2521	10.2205	3.1575E−02
#10	11.0449	0.9880	0.9847	3.2573E−03	10.9124	10.8764	3.5977E−02
#11	11.8018	0.9630	0.9602	2.8113E−03	11.3651	11.3320	3.3179E−02
#12	12.4929	0.9255	0.9239	1.6264E−03	11.5622	11.5419	2.0318E−02
#13	13.1231	0.8725	0.8736	1.0664E−03	11.4499	11.4639	1.3995E−02
#14	13.6983	0.8075	0.8082	7.0271E−04	11.0614	11.0710	9.6259E−03
#15	14.2221	0.7265	0.7285	2.0499E−03	10.3324	10.3615	2.9154E−02
#16	14.6995	0.6345	0.6366	2.1332E−03	9.3268	9.3582	3.1357E−02
#17	15.1346	0.5345	0.5354	9.2719E−04	8.0894	8.1035	1.4033E−02
#18	15.5311	0.4275	0.4282	6.9828E−04	6.6395	6.6504	1.0845E−02
#19	15.8929	0.3185	0.3178	6.5133E−04	5.0619	5.0515	1.0351E−02
#20	16.2229	0.2085	0.2070	1.4929E−03	3.3825	3.3583	2.4219E−02
#21	16.5241	0.1010	0.0976	3.3547E−03	1.6689	1.6135	5.5433E−02
#22	16.7987	−0.0080	−0.0086	5.9067E−04	−0.1344	−0.1443	9.9225E−03
#23	17.0499	−0.1110	−0.1110	2.6203E−05	−1.8925	−1.8921	4.4676E−04
#24	17.2793	−0.2090	−0.2086	3.9120E−04	−3.6114	−3.6046	6.7596E−03
#25	17.4885	−0.3030	−0.3009	2.0724E−03	−5.2990	−5.2628	3.6243E−02
Total		$\sum_{i=1}^{N} \lvert I_{exp} - I_{est} \rvert = 0.042553301825101$			$\sum_{i=1}^{N} \lvert P_{exp} - P_{est} \rvert = 0.452910327208718$		

The presented values are in the standard presentation which is consistent with the literature.

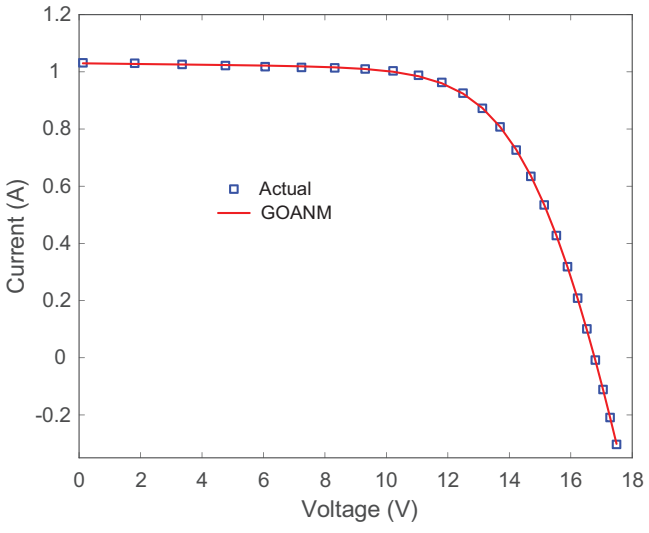


FIGURE 13 Photovoltaic module current-voltage curve characteristics.

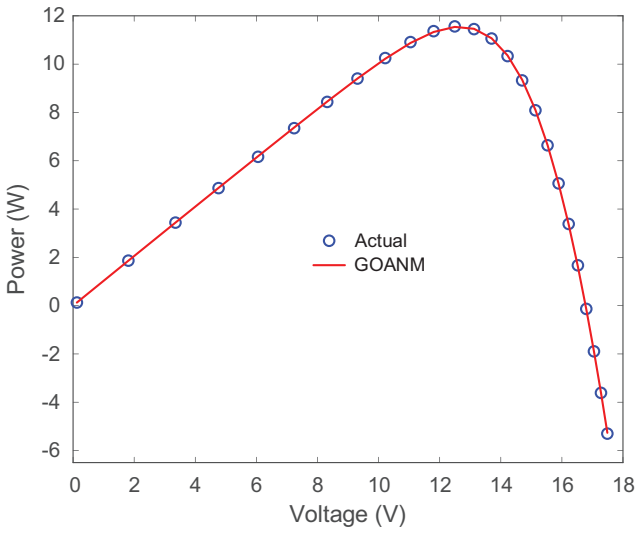


FIGURE 14 Photovoltaic module power-voltage curve characteristics.

17521424, 2024, 6, Downloaded from https://ietresearch.onlinelibrary.wiley.com/doi/10.1049/rpg2.12974 by Turkey Cochrane Evidence Aid, Wiley Online Library on [15/04/2025]. See the Terms and Conditions (https://onlinelibrary.wiley.com/terms-and-conditions) on Wiley Online Library for rules of use; OA articles are governed by the applicable Creative Commons License

TABLE 16 Photovoltaic module estimated parameters and root mean square error values (Photowatt-PWP201).

Approach	I_{ph} (A)	I_{sd} (μA)	R_s (Ω)	R_{sh} (Ω)	n	*RMSE*
GOANM (proposed)	1.0314	2.6380	1.2356	821.6098	47.5981	**2.0528E−03**
GOA (proposed)	1.0299	3.2783	1.2127	1046.5867	48.4076	2.1097E−03
CCNMGBO [41]	1.0305	3.48	1.2013	981.9819	48.6428	2.4251E−03
IMFOL [42]	1.0305	3.5151	1.2003	992.2601	48.6788	2.4252E−03
RTLBO [43]	1.0305	3.4823	1.2013	981.9822	48.6428	2.4251E−03
DLMVO [45]	1.0305	3.4822	1.2013	981.9823	48.6428	2.4251E−03
OBL-RSACM [46]	1.0305	3.8423	1.2009	983.7382	48.5955	2.4251E−03
CGO-LS [47]	1.0305	3.4823	1.2013	981.9822	48.6428	2.4251E−03
AHO [48]	1.0314	2.6381	1.2356	821.6413	46.7172	2.2953E−03
PSOCS [49]	1.0305	3.4823	1.2013	981.98	48.643	2.4251E−03
ELADE [50]	1.0305	3.4823	1.2013	981.9820	48.6428	2.4251E−03
COA [51]	1.0315	3.6250	1.1979	940.0157	50.7082	2.9496E−03
SDGBO [44]	1.0305	3.4823	1.2013	981.998	48.6429	2.4251E−03
IHGS [52]	1.03051	3.4822	1.2013	981.9505	48.6428	2.4251E−03
BES [53]	1.0305	3.4823	1.2013	981.9824	48.6428	2.4251E−03
DE [56]	1.0314	2.6380	1.2348	821.6568	47.3004	2.0529E−03
ITSA [54]	1.0318	3.2840	1.2056	841.321	48.4036	2.427E−03
TSA [55]	1.0311	3.4670	1.2004	912.4803	48.6286	2.4326E−03

The presented values are in the standard presentation which is consistent with the literature.

excels in parameter estimation for the SDM and DDM of the RTC France solar cell and the Photowatt-PWP201 PV module. Comparative analysis highlights its superiority, emphasizing the potential for practical application. The GOANM algorithm exhibited faster convergence, smoother convergence behaviour, and close agreement between experimental and estimated values. The *I–V* and *P–V* curve characteristics of the optimized models closely matched the experimental data. Comparative analysis with other recent optimization approaches further highlighted the superior performance of the GOANM algorithm, as it achieved the lowest RMSE values among all the methods considered. Future research avenues include extending GOANM to diverse PV models, evaluating its adaptability in various environmental scenarios, exploring hybridization with other algorithms, and incorporating uncertainty analysis for real-world reliability assessments.

AUTHOR CONTRIBUTIONS

Serdar Ekinci: Conceptualization; data curation; formal analysis; investigation; methodology; software; validation; visualization; writing—original draft. **Davut Izci**: Conceptualization; data curation; formal analysis; investigation; methodology; project administration; software; writing—original draft. **Abdelazim G. Hussien**: Investigation; validation; writing—review and editing; project administration.

CONFLICT OF INTEREST STATEMENT

The authors declare no conflicts of interest.

DATA AVAILABILITY STATEMENT

Data is available based on a reasonable request.

ORCID

Serdar Ekinci https://orcid.org/0000-0002-7673-2553
Davut Izci https://orcid.org/0000-0001-8359-0875
Abdelazim G. Hussien https://orcid.org/0000-0001-5394-0678

REFERENCES

1. Gani, A.: Fossil fuel energy and environmental performance in an extended STIRPAT model. J. Cleaner Prod. 297, 126526 (2021)
2. Hassan, A., Ilyas, S.Z., Jalil, A., Ullah, Z.: Monetization of the environmental damage caused by fossil fuels. Environ. Sci. Pollut. Res. Int. 28(17), 21204–21211 (2021)
3. Cho, J.H., Sohn, S.Y.: A novel decomposition analysis of green patent applications for the evaluation of R&D efforts to reduce CO_2 emissions from fossil fuel energy consumption. J. Cleaner Prod. 193, 290–299 (2018)
4. Baloch, Z.A., Tan, Q., Kamran, H.W., Nawaz, M.A., Albashar, G., Hameed, J.: A multi-perspective assessment approach of renewable energy production: policy perspective analysis. Environ. Dev. Sustainability 24(2), 2164–2192 (2022)
5. Bakır, H.: Comparative performance analysis of metaheuristic search algorithms in parameter extraction for various solar cell models. Environ. Challenges 11, 100720 (2023)
6. Sayed, A., El-Shimy, M., El-Metwally, M., Elshahed, M.: Reliability, availability and maintainability analysis for grid-connected solar photovoltaic systems. Energies 12(7), 1213 (2019)
7. Abdelrazik, A.S., Al-Sulaiman, F., Saidur, R., Ben-Mansour, R.: A review on recent development for the design and packaging of hybrid photovoltaic/thermal (PV/T) solar systems. Renewable Sustainable Energy Rev. 95, 110–129 (2018)

17521424, 2024, 6, Downloaded from https://ietresearch.onlinelibrary.wiley.com/doi/10.1049/rpg2.12974 by Turkey Cochrane Evidence Aid, Wiley Online Library on [15/04/2025]. See the Terms and Conditions (https://onlinelibrary.wiley.com/terms-and-conditions) on Wiley Online Library for rules of use; OA articles are governed by the applicable Creative Commons License

8. Tyagi, V.V., Chopra, K., Kalidasan, B., et al.: Phase change material based advance solar thermal energy storage systems for building heating and cooling applications: A prospective research approach. Sustainable Energy Technol. Assess. 47, 101318 (2021)
9. Izci, D., Ekinci, S., Hussien, A.G.: Effective PID controller design using a novel hybrid algorithm for high order systems. PLoS One 18(5), e0286060 (2023)
10. Izci, D., Ekinci, S., Budak, C., Gider, V.: PID controller design for DFIG-based wind turbine via reptile search algorithm. In: 2022 Global Energy Conference (GEC). Batman, Turkey, pp. 154–158. (2022)
11. Izci, D., Ekinci, S., Dal, S., Sezgin, N.: Parameter estimation of solar cells via weighted mean of vectors algorithm. In: 2022 Global Energy Conference (GEC). Batman, Turkey, pp. 312–316. (2022)
12. Premkumar, M., Jangir, P., Sowmya, R.: Parameter extraction of three-diode solar photovoltaic model using a new metaheuristic resistance–capacitance optimization algorithm and improved Newton–Raphson method. J. Comput. Electron. 22, 439–470 (2022)
13. Premkumar, M., Jangir, P., Kumar, C., et al.: Constraint estimation in three-diode solar photovoltaic model using Gaussian and Cauchy mutation-based hunger games search optimizer and enhanced Newton–Raphson method. IET Renewable Power Gener. 16(8), 1733–1772 (2022)
14. Rizk-Allah, R.M., El-Fergany, A.A.: Conscious neighborhood scheme-based Laplacian barnacles mating algorithm for parameters optimization of photovoltaic single- and double-diode models. Energy Convers. Manag. 226, 113522 (2020)
15. Manoharan, P., Ravichandran, S., Jangir, P.: ZRMSE: A new and reliable approach for computing the circuit parameters of single-diode solar photovoltaic model. In: 2022 IEEE 2nd International Conference on Sustainable Energy and Future Electric Transportation (SeFeT). Hyderabad, India, pp. 1–7 (2022)
16. Ahmadianfar, I., Gong, W., Heidari, A.A., Golilarz, N.A., Samadi-Koucheksaraee, A., Chen, H.: Gradient-based optimization with ranking mechanisms for parameter identification of photovoltaic systems. Energy Rep. 7, 3979–3997 (2021)
17. Xu, B., Heidari, A.A., Kuang, F., Zhang, S., Chen, H., Cai, Z.: Performance optimization of photovoltaic systems: Reassessment of political optimization with a quantum Nelder-mead functionality. Sol. Energy 234, 39–63 (2022)
18. Maden, D., Çelik, E., Houssein, E.H., Sharma, G.: Squirrel search algorithm applied to effective estimation of solar PV model parameters: a real-world practice. Neural. Comput. Appl. 35(18), 13529–13546 (2023)
19. Long, W., Wu, T., Xu, M., Tang, M., Cai, S.: Parameters identification of photovoltaic models by using an enhanced adaptive butterfly optimization algorithm. Energy 229, 120750 (2021)
20. Touabi, C., Ouadi, A., Bentarzi, H.: Photovoltaic panel parameters estimation using an opposition based initialization particle swarm optimization. In: The 2nd International Conference on Computational Engineering and Intelligent Systems. p. 16 (2023)
21. Duan, Z., Yu, H., Zhang, Q., Tian, L.: Parameter extraction of solar photovoltaic model based on nutcracker optimization algorithm. Appl. Sci. 13(11), 6710 (2023)
22. Duman, S., Kahraman, H.T., Sonmez, Y., Guvenc, U., Kati, M., Aras, S.: A powerful meta-heuristic search algorithm for solving global optimization and real-world solar photovoltaic parameter estimation problems. Eng. Appl. Artif. Intell. 111, 104763 (2022)
23. Aribia, H. Ben, El-Rifaie, A.M., Tolba, M.A., et al.: Growth optimizer for parameter identification of solar photovoltaic cells and modules. Sustainability 15(10), 7896 (2023)
24. Yang, C., Su, C., Hu, H., Habibi, M., Safarpour, H., Amine Khadimallah, M.: Performance optimization of photovoltaic and solar cells via a hybrid and efficient chimp algorithm. Sol. Energy 253, 343–359 (2023)
25. Garip, Z.: Parameters estimation of three-diode photovoltaic model using fractional-order Harris Hawks optimization algorithm. Optik 272, 170391 (2023)
26. Premkumar, M., Shankar, N., Sowmya, R., et al.: A reliable optimization framework for parameter identification of single-diode solar photovoltaic model using weighted velocity-guided grey wolf optimization algorithm and Lambert-W function. IET Renewable Power Gener. 17, 2711-2732 (2023)
27. Madhiarasan, M., Cotfas, D.T., Cotfas, P.A.: Black widow optimization algorithm used to extract the parameters of photovoltaic cells and panels. Mathematics 11(4), 967 (2023)
28. Houssein, E.H., Zaki, G.N., Diab, A.A.Z., Younis, E.M.G.: An efficient Manta Ray Foraging Optimization algorithm for parameter extraction of three-diode photovoltaic model. Communist Chin. Sci. Abstr. 94, 107304 (2021)
29. Moustafa, G.: Parameter identification of solar photovoltaic systems using an augmented subtraction-average-based optimizer. Eng 4(3), 1818–1836 (2023)
30. Premkumar, M., Jangir, P., Elavarasan, R.M., Sowmya, R.: Opposition decided gradient-based optimizer with balance analysis and diversity maintenance for parameter identification of solar photovoltaic models. J. Ambient Intell. Hum. Comput. 14(6), 7109–7131 (2023)
31. Premkumar, M., Jangir, P., Sowmya, R., Elavarasan, R.M., Kumar, B.S.: Enhanced chaotic JAYA algorithm for parameter estimation of photovoltaic cell/modules. ISA Trans. 116, 139–166 (2021)
32. Premkumar, M., Jangir, P., Ramakrishnan, C., Nalinipriya, G., Alhelou, H.H., Kumar, B.S.: Identification of solar photovoltaic model parameters using an improved gradient-based optimization algorithm with chaotic drifts. IEEE Access 9, 62347–62379 (2021)
33. Premkumar, M., Sowmya, R., Umashankar, S., Jangir, P.: Extraction of uncertain parameters of single-diode photovoltaic module using hybrid particle swarm optimization and grey wolf optimization algorithm. Mater. Today Proc. 46, 5315–5321 (2021)
34. Premkumar, M., Sowmya, R., Jangir, P., Kumar, J.S.V.S.: A new and reliable objective functions for extracting the unknown parameters of solar photovoltaic cell using political optimizer algorithm. In: 2020 International Conference on Data Analytics for Business and Industry: Way Towards a Sustainable Economy (ICDABI). pp. 1–6 (2020)
35. Zheng, R., Hussien, A.G., Qaddoura, R., et al.: A multi-strategy enhanced African vultures optimization algorithm for global optimization problems. J. Comput. Des. Eng. 10(1), 329–356 (2023)
36. Sasmal, B., Hussien, A.G., Das, A., Dhal, K.G.: A comprehensive survey on aquila optimizer. Arch. Comput. Meth. Eng. 30(7), 4449–4476 (2023)
37. Hashim, F.A., Hussien, A.G.: Snake optimizer: A novel meta-heuristic optimization algorithm. Knowledge-Based Syst. 242, 108320 (2022)
38. Hashim, F.A., Mostafa, R.R., Hussien, A.G., Mirjalili, S., Sallam, K.M.: Fick's Law Algorithm: A physical law-based algorithm for numerical optimization. Knowledge-Based Syst. 260, 110146 (2023)
39. Izci, D., Ekinci, S.: A novel hybrid ASO-NM algorithm and its application to automobile cruise control system. In: 2nd International Conference on Artificial Intelligence: Advances and Applications. pp. 333–343 (2022)
40. Agushaka, J.O., Ezugwu, A.E., Abualigah, L.: Gazelle optimization algorithm: a novel nature-inspired metaheuristic optimizer. Neural. Comput. Appl. 35, 4099–4131 (2023)
41. Premkumar, M., Jangir, P., Ramakrishnan, C., et al.: An enhanced gradient-based optimizer for parameter estimation of various solar photovoltaic models. Energy Rep. 8, 15249–15285 (2022)
42. Qaraad, M., Amjad, S., Hussein, N.K., Badawy, M., Mirjalili, S., Elhosseini, M.A.: Photovoltaic parameter estimation using improved moth flame algorithms with local escape operators. Comput. Electr. Eng. 106, 108603 (2023)
43. Yu, X., Hu, Z., Wang, X., Luo, W.: Ranking teaching–learning-based optimization algorithm to estimate the parameters of solar models. Eng. Appl. Artif. Intell. 123, 106225 (2023)
44. Yu, S., Chen, Z., Heidari, A.A., Zhou, W., Chen, H., Xiao, L.: Parameter identification of photovoltaic models using a sine cosine differential gradient based optimizer. IET Renewable Power Gener. 16(8), 1535–1561 (2022)
45. Li, J., Dang, J., Xia, C., et al.: Dynamic leader multi-verse optimizer (DLMVO): A new algorithm for parameter identification of solar PV models. Appl. Sci. 13(9), 5751 (2023)
46. Chauhan, S., Vashishtha, G., Kumar, A.: Approximating parameters of photovoltaic models using an amended reptile search algorithm. J. Ambient Intell. Hum. Comput. 14(7), 9073–9088 (2023)

17521424, 2024, 6, Downloaded from https://ietresearch.onlinelibrary.wiley.com/doi/10.1049/rpg2.12974 by Turkey Cochrane Evidence Aid, Wiley Online Library on [15/04/2025]. See the Terms and Conditions (https://onlinelibrary.wiley.com/terms-and-conditions) on Wiley Online Library for rules of use; OA articles are governed by the applicable Creative Commons License

47. Bogar, E.: Chaos game optimization-least squares algorithm for photovoltaic parameter estimation. Arab. J. Sci. Eng. 48(5), 6321–6340 (2023)
48. Ayyarao, T.S.L.V., Kishore, G.I.: Parameter estimation of solar PV models with artificial humming bird optimization algorithm using various objective functions. Soft Comput. 28, 3371–3392 (2024)
49. Fan, Y., Wang, P., Heidari, A.A., Chen, H., HamzaTurabieh, Mafarja, M.: Random reselection particle swarm optimization for optimal design of solar photovoltaic modules. Energy 239, 121865 (2022)
50. Gu, Z., Xiong, G., Fu, X., et al.: Extracting accurate parameters of photovoltaic cell models via elite learning adaptive differential evolution. Energy Convers. Manag. 285, 116994 (2023)
51. Diab, A.A.Z., Sultan, H.M., Do, T.D., Kamel, O.M., Mossa, M.A.: Coyote optimization algorithm for parameters estimation of various models of solar cells and PV modules. IEEE Access 8, 111102–111140 (2020)
52. Xu, B., Heidari, A.A., Kuang, F., Zhang, S., Chen, H., Cai, Z.: Quantum Nelder-Mead hunger games search for optimizing photovoltaic solar cells. Int. J. Energy Res. 46(9), 12417–12466 (2022)
53. Nicaire, N.F., Steve, P.N., Salome, N.E., Grégroire, A.O.: Parameter estimation of the photovoltaic system using bald eagle search (BES) algorithm. Int. J. Photoenergy 2021, 1–20 (2021)
54. Arandian, B., Eslami, M., Khalid, S.A., et al.: An effective optimization algorithm for parameters identification of photovoltaic models. IEEE Access 10, 34069–34084 (2022)
55. Beşkirli, A., Dağ, İ.: An efficient tree seed inspired algorithm for parameter estimation of photovoltaic models. Energy Rep. 8, 291–298 (2022)
56. Kharchouf, Y., Herbazi, R., Chahboun, A.: Parameter's extraction of solar photovoltaic models using an improved differential evolution algorithm. Energy Convers. Manag. 251, 114972 (2022)
57. Karatzas, I., Shreve, S.E.: Brownian Motion. In: Brownian Motion and Stochastic Calculus. Graduate Texts in Mathematics, vol 113. Springer, New York, NY (1998). https://doi.org/10.1007/978-1-4612-0949-2_2
58. Izci, D., Ekinci, S., Mirjalili, S., Abualigah, L.: An intelligent tuning scheme with a master/slave approach for efficient control of the automatic voltage regulator. Neural Comput. Appl. 35(26), 19099–19115 (2023)
59. Mantegna, R.N.: Fast, accurate algorithm for numerical simulation of Lévy stable stochastic processes. Phys. Rev. E 49(5), 4677–4683 (1994)
60. Izci, D.: Design and application of an optimally tuned PID controller for DC motor speed regulation via a novel hybrid Lévy flight distribution and Nelder–Mead algorithm. Trans. Inst. Meas. Control 43(14), 3195–3211 (2021)
61. Olson, K.A., Larsen, E.A., Mueller, T., et al.: Survival probabilities of adult Mongolian gazelles. J. Wildl. Manage. 78(1), 35–41 (2014)
62. Lagarias, J.C., Reeds, J.A., Wright, M.H., Wright, P.E.: Convergence properties of the Nelder-Mead simplex method in low dimensions. SIAM J. Optim. 9(1), 112–147 (1998)
63. Rajan, A., Malakar, T.: Optimal reactive power dispatch using hybrid Nelder-Mead simplex based firefly algorithm. Int. J. Electr. Power Energy Syst. 66, 9–24 (2015)
64. Senthil Kumar, J., Charles Raja, S., Jeslin Drusila Nesamalar, J., Venkatesh, P.: Optimizing renewable based generations in AC/DC microgrid system using hybrid Nelder-Mead – Cuckoo Search algorithm. Energy 158, 204–215 (2018)
65. Yildiz, A.R.: A novel hybrid whale–Nelder–Mead algorithm for optimization of design and manufacturing problems. Int. J. Adv. Manuf. Technol. 105(12), 5091–5104 (2019)
66. Chen, C., Yu, L.: A hybrid ant lion optimizer with improved Nelder–Mead algorithm for structural damage detection by improving weighted trace lasso regularization. Adv. Struct. Eng. 23(3), 468–484 (2020)
67. Izci, D., Hekimoğlu, B., Ekinci, S.: A new artificial ecosystem-based optimization integrated with Nelder-Mead method for PID controller design of buck converter. Alexandria Eng. J. 61(3), 2030–2044 (2022)
68. Ekinci, S., Izci, D., Abualigah, L.: A novel balanced Aquila optimizer using random learning and Nelder–Mead simplex search mechanisms for air–fuel ratio system control. J. Braz. Soc. Mech. Sci. Eng. 45(1), 68 (2023)
69. Izci, D., Ekinci, S.: A novel improved version of hunger games search algorithm for function optimization and efficient controller design of buck converter system. e-Prime—Adv. Electr. Eng. Electron. Energy 2, 100039 (2022)
70. Özmen, H., Ekinci, S., Izci, D.: Boosted arithmetic optimization algorithm with elite opposition-based pattern search mechanism and its promise to design microstrip patch antenna for WLAN and WiMAX. Int. J. Model. Simul. 1–16 (2023)
71. Ekinci, S., Izci, D., Abu Zitar, R., Alsoud, A.R., Abualigah, L.: Development of Lévy flight-based reptile search algorithm with local search ability for power systems engineering design problems. Neural Comput. Appl. 34(22), 20263–20283 (2022)
72. Snášel, V., Rizk-Allah, R.M., Izci, D., Ekinci, S.: Weighted mean of vectors optimization algorithm and its application in designing the power system stabilizer. Appl. Soft Comput. 136, 110085 (2023)
73. Ayyarao, T.S.L.V.: Parameter estimation of solar PV models with quantum-based avian navigation optimizer and Newton–Raphson method. J. Comput. Electron. 21(6), 1338–1356 (2022)

How to cite this article: Ekinci, S., Izci, D., Hussien, A.G.: Comparative analysis of the hybrid gazelle-Nelder–Mead algorithm for parameter extraction and optimization of solar photovoltaic systems. IET Renew. Power Gener. 18, 959–978 (2024). https://doi.org/10.1049/rpg2.12974

17521424, 2024, 6, Downloaded from https://ietresearch.onlinelibrary.wiley.com/doi/10.1049/rpg2.12974 by Turkey Cochrane Evidence Aid, Wiley Online Library on [15/04/2025]. See the Terms and Conditions (https://onlinelibrary.wiley.com/terms-and-conditions) on Wiley Online Library for rules of use; OA articles are governed by the applicable Creative Commons License